Supplementary Materials for

Prefrontal cortical regulation of brainwide circuit dynamics and reward-related behavior

Emily A. Ferenczi, Kelly A. Zalocusky, Conor Liston, Logan Grosenick, Melissa R. Warden, Debha Amatya, Kiefer Katovich, Hershel Mehta, Brian Patenaude, Charu Ramakrishnan, Paul Kalanithi, Amit Etkin, Brian Knutson, Gary H. Glover, Karl Deisseroth*

*Corresponding author. E-mail: deissero@stanford.edu

Published 1 January 2016, *Science* **351**, aac9698 (2016)
DOI: 10.1126/science.aac9698

This PDF file includes:

Other Supplementary Material for this manuscript includes the following:

Data S1 (as a zipped archive): available at http://clarityresourcecenter.org/ofMRI.html

Materials and Methods

All experiments conformed to guidelines established by the National Institutes of Health and were conducted under protocols approved by the Stanford Administrative Panel on Laboratory Animal Care.

Subjects

Female Long-Evans TH-Cre rats (200-300 grams at time of surgery) were bred in-house (*30*). Wild-type male Sprague Dawley rats (250-400 grams at time of surgery) were obtained from Charles River. Rats were pair housed on a standard 12 hour light-dark cycle and given food and water ad libitum.

Virus packaging

Recombinant AAV vectors were serotyped with AAV5 coat proteins and produced by the vector core at the University of North Carolina. Viral titres (in particles/mL) were 1 x 10^{13} for AAV5-EF1α-DIO-ChR2(H134R)-eYFP, 4 x 10^{12} for AAV5-EF1α-DIO-eYFP, 1.5-4.8 x 10^{12} for AAV5-EF1α-DIO-eNpHR3.0-eYFP, 4 x 10^{12} for AAV5-EF1α-DIO-C1V1$_{TT}$-eYFP, 2-4 x 10^{12} for AAV5-CKIIα-SSFO-eYFP, 6 x 10^{12} for AAV5-CKIIα-eYFP. Maps are available online from www.optogenetics.org.

Stereotactic surgeries

All stereotactic surgeries were performed with rats (8-10 weeks of age) under isoflurane anesthesia (4% initially, maintained at 2-3%) with regular monitoring for stable respiratory rate and absent tail pinch response. The scalp was shaved and rats were placed in the stereotactic apparatus with non-rupturing ear bars. A heating pad was used to prevent hypothermia. Rats were administered with lactated Ringer's solution (5mL/kg subcutaneous), buprenorphine (0.05 mg/kg subcutaneous), enrofloxacin (5 mg/kg, subcutaneous). A midline incision was made to expose the skull and craniotomies were made unilaterally. Virus injections were delivered with a 10 μL syringe and 33 gauge beveled needle injected at 100 nL/min using an injection pump. Following injection, the injection needle was held at the injection site for 10 mins then slowly withdrawn. The skull was then prepared for implantation of a custom-made MRI-compatible

head post with three "feet" on its undersurface, to provide traction with the skull (clear Perspex, manufactured by the Physics Machine Shop, Stanford University). The skull was cleaned and 3 non-invasive invaginations in the skull were made in a triangular formation in front of bregma for the "feet" of the head post. The head post secured the head position relative to the MRI-compatible cradle during MRI habituation and scanning. A 300 μm 0.37 NA optical fiber (ceramic ferrule, Doric Lenses and ThorLabs) was cut to length and inserted through the craniotomy at the site of virus injection. The fiber was secured in place with dental cement (Metabond® clear L-powder, Parkell, Inc., Edgewood, NY). The Perspex head post was then lowered into position, and similarly secured in place. Additional dental cement was then applied to further secure both the fiber and head post to each other and the skull. The skin was then sutured closed and the rats recovered under a heated lamp. Virus was allowed to express for a minimum of 4 weeks before stimulation experiments were initiated.

Coordinates for injections and fiber implantation

To target medial prefrontal cortex pyramidal neurons SSFO, a single 1 μL injection was made at AP + 2.7, ML 0.5 (right), DV 5.0 (predominantly targeting the infralimbic (IL) cortex). Coordinates for fiber implantation in the medial prefrontal cortex were AP + 2.7, ML 0.5 (right), DV 4.8. To target midbrain dopamine neurons with ChR2, eNpHR3.0 or $C1V1_{TT}$, 4 x 1 μL injections were made at the following coordinates: AP -5.4, ML 0.7 (right), DV 7 and 8.2 and AP -6.2, ML 0.7 (right), DV 7 and 8.2. Coordinates for fiber implantation in the midbrain were AP -5.8, ML 0.7 (right), DV 7.3.

For dual stimulation experiments, fiber implantation was performed so as to achieve the same fiber tip locations as specified above, however angled surgeries were necessary to allow for sufficient space on the skull for the head post. Therefore, midbrain and mPFC fibers were implanted at 20° angles (along the AP dimension, with fiber tips angled towards the center of the brain) and the new sites for AP entry to the skull and depth of the fiber were calculated using standard trigonometry. Dual fiber surgeries required approximately 6-7 hours per rat.

Implantation of multi-electrode arrays

For implantation of 24-electrode arrays for in vivo awake electrophysiology, we followed procedures described previously (*88*). Rats were injected with AAV5-CKIIα-SSFO-eYFP at 8-10 weeks and virus was allowed to express for 6-8 weeks before electrode implantation with two 24-electrode arrays with 50 μm stainless steel electrodes. One of the arrays additionally included a 300 μm 0.37 NA optical fiber at its center. Surgical preparation was performed as described above. The skull surface was thoroughly cleaned and ~ 10 skull screws were implanted at the periphery of the skull to stabilize the arrays and the recordings. Two 2-3 mm diameter craniotomies were drilled, one over the medial prefrontal cortex and one over the ventromedial striatum. The array containing the optical fiber was lowered through the medial prefrontal cortex craniotomy (AP +2.7, ML 0.5-1.0, DV 5.0) and the second array was lowered through the striatal craniotomy (AP +0.7 to -0.4, ML 0.5-1.5, DV 5.0-6.0). The electrode arrays were secured to the skull and the screws using dental acrylic. The skin was sutured closed and the rats allowed to recover as described above.

Behavioral experiments

Operant chamber self-stimulation

Operant chamber behavioral testing was performed as described previously (*30*). In brief, TH-Cre rats were trained in 1 to 2 hour sessions daily for 2 to 4 days in which they could respond freely at two lever pressing ports. A response at the active port delivered a 1 s train of light pulses (20 Hz, 20 pulses, 5 ms pulse width, peak light power of 1.5 - 2 mW at the fiber tip, after correction for the duty cycle). Responses at the inactive port were without consequence. The number of responses at each port was recorded. Results were analyzed using GraphPad Prism software. Dose-response experiments using operant nose-poke self-stimulation behavior were performed as described previously (*30*) to establish the optimal stimulation duration for subsequent MRI experiments.

Real-time place preference

Real-time place preference was performed using a three-chamber apparatus (as depicted in Fig. 6g and Fig. S7b), with two large chambers separated by a small central chamber and rats were allowed to roam freely between all three compartments. The large chambers had different visual appearances, one with black spots on white walls and one with black stripes on white walls.

Optogenetic stimulation was delivered only when the rat entered one of the chambers (the contingent chamber was designated in advance). For dopaminergic inhibition experiments eNpHR3.0-mediated inhibition was delivered using 590 nm continuous light (~10 mW at fiber tip). For dual stimulation experiments, $C1V1_{TT}$-mediated dopamine neuron stimulation was delivered using 590 nm, 20 Hz pulses, 5 ms pulse width (15 mW at fiber tip). When the rat chose to leave the designated optogenetic stimulation chamber, light stimulation was terminated. Video monitoring was performed to assess the duration of time spent in each chamber (for a within-animal comparison). For eNpHR3.0 experiments, the total test duration was 15 mins. For dual stimulation experiments, the test was divided into three 10 minute epochs, with the first 10 minutes serving as a baseline epoch in which only $C1V1_{TT}$ stimulation was delivered, contingent on the rat entering the designated chamber. The middle 10 minute epoch included superimposed mPFC SSFO stimulation, with the delivery of a single pulse of blue light (470 nm, 5 s continuous, 5 mW at fiber tip) to the mPFC at the start of the 10 minutes, and a single pulse of yellow light (590 nm, 10 s continuous, 15 mW at fiber tip) at the end of the 10 minutes for all rats, with $C1V1_{TT}$ stimulation still contingent on entry to the designated chamber as before. The final 10 minutes served as a "washout" or recovery epoch, in which $C1V1_{TT}$ stimulation was delivered on chamber entry, as during the baseline epoch, with no SSFO stimulation.

Sucrose preference

Rats were moved to a reverse light-dark cycle housing facility 3 days prior to testing and were manually handled daily to accustom them to human handling prior to the first experimental day. The experimenter was blinded to the identity of SSFO and YFP rats. Rats were habituated to the presence of two drinking bottles in their cages. On the first day both bottles contained plain water, on the second day both bottles contained a 1% sucrose (Sigma Aldrich) solution dissolved in the rats' normal drinking water. Rats had access to food and water ad libitum. After 3 days of handling and habituation, sucrose preference testing began. The sucrose preference test (SPT) started at 8 am and ended at 2pm. During this period the rats had free access to the choice of plain water or 1% sucrose. The bottles containing the two solutions were weighed at the start and end of the testing period. At the end of the testing period, the sucrose and water bottles were removed and the rats were provided with their usual water bottles. For baseline days 1 & 2, a fiber optic patch cord (unconnected to a laser) was attached via a zirconia sleeve to each rats'

optical fiber implant at the start of the testing session for 5 s and then removed, with no light having been delivered. This was repeated 4 times (approximately 1 to 1.5 hour intervals) throughout the 6-hour testing period. For test days 3 to 8 (light stimulation days), the fiber optic patch cord was attached as for the baseline days but this time delivered a 5 second pulse of 470 nm light (6 mW at the fiber tip) from a 470 nm diode controlled by a diode pumped solid state laser (OEM Laser Systems, Inc., Salt Lake City, UT), controlled by a Master-8 stimulus generator (A.M.P.I. Jerusalem, Israel), repeated 4 times over the course of the 6 hour testing period. For recovery days 9 to 12, sham stimulation (as for the baseline period) was performed (handling and fiber attachment but no light delivery). Total sucrose consumption, total water consumption and total fluid consumption were recorded daily. Sucrose preference for each test day was calculated as:

Sucrose preference (%) = (sucrose consumption / (sucrose + water consumption)) * 100

Results were analyzed using Microsoft Excel and GraphPad Prism software. Exclusion criteria: rats were excluded if baseline sucrose preference was < 70%. This criterion, which resulted in the exclusion of 1 rat from the experiment, was decided upon prior to the commencement of behavioral testing. One rat was also excluded due to the occurrence of seizures on light delivery.

Social interaction

In the social interaction test, animals were handled for three days at baseline before the introduction of a same-sex (male) juvenile into their home cage for a period of 2 minutes, during which time the social investigation of the juvenile was monitored and timed. Rats were then exposed to three days of chronic mPFC SSFO stimulation with blue light (4 pulses per day, 470 nm, 5 s continuous, 5-6 mW at fiber tip) and a social interaction test (with the same juvenile) was repeated on the third day. This was followed by a recovery or "washout" period of three days, with daily handling but no light stimulation, ending with a third and final social interaction test (with the same juvenile). The same juvenile was used in each test to minimize variability due to juvenile differences. All tests were conducted in low-normal room light, allowing sufficient light for video monitoring. This experimental design was also used to assess exploration of a novel object and locomotion in the open field (Fig. 4l). For novel object testing, a novel object was introduced into the home cage for 2 minutes and investigation of the object was monitored and

timed. The open field chamber was a large black box, (80 cm length, 45 cm width, 40 cm height), and was cleaned with 70% ethanol between each rat. Locomotion was monitored for 10 minutes in each phase of the test. As before, the experiments were performed at baseline (after three days of handling), with chronic light stimulation (three days of light stimulation (4 pulses of blue light/day) and after a washout period (three days of handling, no light stimulation). The experimenter was blinded to the identity of SSFO and YFP rats in all experiments. In between social behavior testing and novel object/locomotion testing, one SSFO-expressing subject died of unknown causes.

MRI compatible head fixation and habituation procedure

The MRI-compatible bed, restraint system and MRI simulation environment are depicted in Figure 1a and Fig. S1. Rats were surgically implanted with a custom-made Perspex head post with three "feet" on its undersurface, which provided traction with the skull. The upper surface of the head post contained three 4/40 screw holes which allowed the head piece to be secured to a Perspex arch piece which then attached to the MRI-compatible bed. The head post secured the head position relative to the MRI-compatible cradle during MRI habituation and scanning.

Habituation began at least 4 weeks after any surgical procedure. Rats were habituated to the MRI environment in a progressive manner to minimize stress associated with awake scanning (*89*). An "MRI simulation environment" was created consisting of a black, 45 cm length, 12 cm diameter "bore" in which the Perspex MRI bed could be inserted with several centimeters clearance between the rat's head and the top of the bore. Rats were anaesthetized briefly (less than 10 minutes) to allow placement in the MRI environment with a nylon and canvas restraint system (Snuggle, Harvard Apparatus) and attachment of the head post to the MRI arch piece with plastic screws. Rats were then allowed to emerge from anesthesia while in the simulation environment. Sounds recorded directly from the scanner during a functional scan were replayed to the rat through a small speaker set situated close to the bore. Rats were continually monitored by an experimenter throughout the entire habituation procedure. Duration of exposure to the habituation environment began at 5 minutes or less on the first day of training, progressively increasing in duration by 5-10 minutes with each day of habituation, until a total of 40-45 minutes with minimal motion was achieved without evidence of distress (5-10 days). If animals

showed signs of struggling or distress they were immediately anesthetized and removed from the habituation environment. At the end of each habituation day, the rats were rewarded with a sugary treat (Fruity O's, Trader Joes, Inc., and white chocolate chips, Whole Foods Market, Inc.).

Magnetic resonance imaging

A number of key technical refinements allowed us to more readily visualize BOLD responses to a variety of stimuli. First, to scan awake rodents, we constructed a customized MRI compatible head fixation apparatus and habituated rats to the scanner environment to minimize stress and motion (as described above). Second, we optimized fast single-shot (0.5 s TR; spiral-in/out) image acquisition protocols (*85*), which minimized motion artifacts from image fusion as well as reduced susceptibility artifacts from implanted material or airspaces in the skull. Third, we used an event-related pseudorandom stimulus sequence, which maximized the number of trials per scan, while still affording resolution of phasic responses to optogenetic stimulation. Specifically, the maximum length sequence (m-sequence) design (*86*) allowed simultaneous but non-correlated presentation of two stimuli, such that optogenetic stimulation occurred while a "positive control" stimulus was also applied (i.e., here, a visual stimulus), to allow verification of BOLD responses to sensory input in experiments in which the BOLD response to optogenetic stimulation might be expected to be absent or reduced (e.g. YFP controls, pharmacological manipulations or dual stimulation optogenetic experiments). During pilot testing, we noticed that the hemodynamic response function (HRF) to SSFO and visual stimulation differed from that observed in response to ChR2 stimulation of dopamine neurons and from the HRF commonly observed in humans (*87*). We found that for SSFO and visual stimulation, the HRF more closely followed a customized model, with exponential rise and decay (τ of 7 s; Fig. S15). Although modeling with the canonical human hemodynamic response function replicated our results, the rat-specific model more effectively resolved activity in SSFO and visual experiments. While the hemodynamic responses of different species might vary for a number of reasons (e.g. differences in the properties of rat capillary networks, they may also vary as a function of brain region (e.g. cortical versus subcortical, neurotransmitter release (dopamine versus glutamate) or the eliciting method of stimulation (e.g. ChR2 versus SSFO). Based on these findings, we recommend that investigators closely inspect raw data acquired in ofMRI experiments prior to applying models

optimized for human data, in order to ensure that divergent temporal features of the rat hemodynamic response function are considered.

Small animal scanner and radiofrequency coil

A 7 Tesla magnet (Agilent Discovery MR901) specialized for small animal imaging and a custom-made 2.5 cm single channel surface coil (Ron Watkins, Radiological Sciences Laboratory, Stanford) were used for all scans, which were performed at the Stanford Small Animal Imaging Facility (Sci3), supported by Laura J. Pisani.

Subject preparation

Rats were briefly anesthetized (5-10 mins) for placement in the MRI scanner, using an identical restraint device as described for the MRI simulation environment. Rats were given wax ear plugs, and a respiratory monitor was inserted into the canvas "Snuggle" restraint device (Harvard Apparatus) next to the rat's thorax, for continuous respiratory monitoring. Rats were kept warm with continual flow of warm air. No bite bar was used. The radiofrequency surface coil was secured above the head using micropore tape. One optical fiber (Thorlabs) was attached to the implanted fiber optic using a zirconia sleeve (Thorlabs) for optogenetic light delivery and a second fiber with a diffuser at the tip was placed ~ 1 cm in front of the eye (right eye in most scans, unless space constraints dictated otherwise). Anesthesia was maintained with isoflurane during shimming, the localizer scan, and the T2 anatomy scan. Isoflurane and oxygen were then switched off at the beginning of the functional scans so that each rat transitioned into an awake state. Respiratory rate was monitored continually and served as a marker for when the rats woke up. Motion plots were obtained at the end of each scan (Fig. 1c,d). Total scanning time was approximately 1-1.5 hours (~45 minutes in the awake state). If there was evidence of distress (change in respiratory rate or excessive motion), the scanning procedure was aborted and the rat was immediately removed from the scanner. Rats were rewarded with a sugary treat (Fruity O's, Trader Joes, Inc., and white chocolate chips, Whole Foods Market, Inc.) at the end of the scan.

Scanner- synchronized stimulation and monitoring

E-Prime® software was used to synchronize the scanner trigger, the lasers for light stimulation and the respiratory monitoring recording software. Computers and light delivery systems were

kept outside the magnet and long optical fibers (6 m) were used to deliver light into the bore of the scanner. For optogenetic stimulation, blue light was delivered using a 470 nm diode pumped solid state laser (OEM Laser Systems, Inc., Salt Lake City, UT), measured at the start of scanning as 5-7 mW (depending on the experiment) at the fiber tip (300 μm fiber diameter). Yellow light was delivered using a 590 nm diode pumped solid state laser (OEM Laser Systems, Inc., Salt Lake City, UT), controlled by an optical shutter (Thorlabs) to maintain stable light power (7-10 mW at fiber tip, depending on the experiment). Green light for $C1V1_{TT}$ stimulation was delivered using a 532 nm diode pumped solid state laser (OEM Laser Systems, Inc., Salt Lake City, UT), Visual stimulation was performed using a green 563 nm diode pumped crystal laser (CrystaLaser®, Reno, NV) with the tip of the optical fiber patch cord covered with a diffuser such that the emitted light was < 0.5 mW in intensity, and tested for comfort by the experimenters.

Laser stimulation protocols varied depending upon the particular functional imaging experiment. For all repetitive stimulation ("task") experiments, an event-related protocol was designed using a binary maximum length sequence (m-sequence) such that it was possible to interleave two simultaneous stimuli, a visual stimulus and an optogenetic stimulus. All stimulation trains consisted of 31 epochs, 16 of which contained stimulation, 15 were "off" epochs. ChR2 stimulation of midbrain dopamine neurons used a 2 s burst of 20 Hz blue light pulses, 10 ms pulse width, with at least 11 s of recovery prior to the next stimulation epoch (light power of 6 - 6.5 mW at the fiber tip). SSFO stimulation of medial prefrontal cortex used a 2 s continuous blue light pulse for activation (5-6 mW at the fiber tip) followed 8 s later by a 3 s continuous yellow light pulse for deactivation (10 mW). Dual stimulation experiments consisted of $C1V1_{TT}$ stimulation of dopamine neurons using a 2 s burst of 20 Hz green light pulses, 10 ms pulse width (6-7 mW at the fiber tip, with same timing as for ChR2 stimulation). When SSFO stimulation was superimposed, a 5 s blue light pulse was delivered prior to the start of the scan (5-6 mW) and a yellow light pulse (10 mW) was delivered after the scan had terminated. The visual stimulus consisted of 13 s epochs of 10 Hz flashing green light, 20 ms pulse width. Resting state scans either contained no stimulus or contained a 5 s continuous blue light pulse before the start of the scan (6 mW), and a 10 s yellow light pulse (10 mW) after the scan had terminated.

MRI data acquisition

Anatomical scans

Localizer and high-order shimming scans were performed prior to the acquisition of anatomical images. T2-weighted anatomical scans were obtained at the start of every scanning procedure using a fast spin-echo sequence (TE/TR: 42/7500 ms, 4 averages, 256 x 256 matrix, 3 cm FOV, 15 slices) to obtain a spatial resolution of 0.1172 x 0.1172 mm in-plane and 1 mm slice thickness.

Functional scans

Functional scans were acquired in the same space as the anatomical scans using a T2*-weighted spiral-in/out, single shot, variable density gradient echo pulse sequence (*83*, *85*) (TE/TR: 15/500 ms, 64 x 64 matrix, 3 cm FOV, 15 slices with no gap). The spiral trajectory was slew-rate limited to 2800 T/m/s and peak amplitude of 290 mT/m, providing a readout duration of 8.8 ms. This produced a resolution of 0.47 x 0.47 mm^2 in-plane and a slice thickness of 1 mm. Functional scans were repeated to obtain a total of ~ 6 to 12 runs (403 s per run) per scanning session, if the subject's comfort level permitted (monitored as described above). Head motion was examined after every scan (Fig. S16).

Pharmacological experiments

For midbrain dopamine neuron stimulation experiments with pharmacology, a series of three scans were performed over the course of 3 to 4 days. The first baseline scan was performed as described above with no intervention. The next day, the pharmacological scan was performed using a cocktail of D1 receptor (SCH23390 0.6 mg/kg, Tocris Bioscience) and D2 receptor (raclopride 0.3 mg/kg, Tocris Bioscience) antagonists administered subcutaneously while the subject was still anesthetized, after the anatomical scan was performed, but immediately prior to the commencement of functional imaging. The first functional scan began within 5 minutes of drug administration and functional scanning continued until up to 10 functional scans were acquired. A "washout" experiment was performed 24 to 48 hours after the drug scan, as dictated by the pharmacokinetics of the drugs (*34*, *35*), in which rats received an i.p. injection of a vehicle control (saline/DMSO) immediately prior to the commencement of functional imaging. Scans were then acquired as above.

MRI data analysis

Pre-processing

Analysis was performed using Analysis for Functional NeuroImages (AFNI, NIMH, Bethesda MD; (*90*). Scans were only included in the awake analysis if isoflurane level was 0% and an increase in respiratory rate to > 100 breaths per minute had occurred, as it took several minutes for the rats to transition from the anesthetized to the awake state. For "task"-like analyses (evoked BOLD responses by optogenetic or visual stimulation), only runs in which the root mean square of displacement was < 0.4 mm were included. BOLD activity time courses and volumes were manually inspected to ensure consistent quality. Runs in which BOLD activity excursions were supra-physiological (exceeded four standard deviations from the mean) were excluded, resulting in the inclusion of 57% of all awake scans in the final analysis with a median of 4 scans per subject. Mean (+/- SEM) head motion score (the root mean square of head motion in three dimensions) for all included awake scans was 0.065 +/- 0.003 (SD = 0.05 mm, n = 255), which was similar to that for anesthetized rats (0.062 +/- 0.02, SD = 0.08 mm, n = 30) (Fig. S16e). Head motion for all scans is provided in Fig. S16. Each functional scan was motion corrected, smoothed using a 0.5 mm FMWH Gaussian blur (note voxel size of 0.47 mm), normalized to the average BOLD activity over the entire scan within each voxel, and temporally bandpass filtered using a Fast Fourier Transform (FFT) with high pass of 0.01 Hz and low pass of 0.3 Hz. Functional volumes were manually inspected to ensure alignment of the functional scans to each subject's own anatomical scan. Each subject's anatomical scan was then aligned to a reference scan (manually chosen by the experimenter for high quality) using a twelve parameter affine transformation (scaling, rotation, shear), and the transformation matrix was applied to each functional scan. Aligned images were then manually inspected for consistent positioning, using the fiber insertion site, cortical contours, and other anatomical landmarks as references.

First level: individual general linear model regressions for evoked activity

Midbrain dopamine neuron stimulation

Based on human fMRI visualizations of striatal activity (*64*), we used a single gamma-variate hemodynamic response function (HRF: AFNI GAM waver function), to convolve a boxcar

model that contrasted stimulation (either optogenetic or visual) against the rest of the scan. Visualization of raw activity time courses revealed this function fit a second prominent peak but not an earlier discovered peak in rats' BOLD response (Fig. S3c). We used the convolved gamma-variate function as the "task" regressor in a general linear model to generate our first level contrasts both for dopamine neuron stimulation and inhibition experiments. We performed a general linear model (GLM) regression analysis for each individual run, including the six motion parameters obtained from the motion correction procedure at the pre-processing stage, as regressors in each model. For dual stimulation scans, we took additional steps to control for motion artifacts, by censoring volumes in which root mean squared displacement exceeded 0.15 mm, and regressed on 12 motion parameters (roll, pitch, yaw, translation in 3 dimensions, and the first derivative of each of those six parameters).

Focal BOLD signal at the fiber site was not consistently observed during midbrain dopamine neuron stimulation. Possible explanations for this could include any or a combination of the following: 1) fewer local recurrent synaptic connections within the dopaminergic midbrain (a major driver for BOLD activity), 2) small number of neurons activated at the fiber site relative to the number of neurons modulated by dopamine in terminal regions, or 3) reduced signal in deeper areas of the brain (further away from surface coil), although SNR calculations did not suggest that this could account for the lack of observed effect.

Medial prefrontal cortex SSFO stimulation and visual stimulation

During pilot block design stimulation trials we noted that the hemodynamic response function (HRF) to 30 s stimulation epochs (SSFO stimulation in medial prefrontal cortex or visual stimulation in superior colliculus) had characteristics that differed from the canonical human HRF (*87*) and also differed from rats' striatal BOLD response to midbrain dopaminergic stimulation by ChR2. This response was best fit by an exponential rise and decay with a time constant of 7 s (Fig. S15). We therefore used this data-derived HRF for first-level analyses, convolving this HRF with the stimulation times and using the convolved function as the "task" regressor in a general linear model to generate first level contrasts. We performed a general linear model regression analysis for each individual run, including the six motion parameters

obtained from the motion correction procedure at the pre-processing stage, as regressors in our model.

Second level: group analysis

The fit coefficients for each run obtained from the first level analysis were then entered into a second level group analysis, where individuals were modeled as fixed effects and voxel-wise t-tests were performed to assess the effect of stimulation (either optogenetic or visual) on BOLD activity. T-scores were converted to Z-scores for ease of comparison and interpretation. P-values were corrected for multiple comparisons across the whole brain using a minimum cluster-size threshold ($K > 5$ functional voxels [80 transformed voxels], uncorrected p-value < 0.01), which was determined on the basis of Monte-Carlo simulation of a random field of noise to ensure an overall alpha probability of < 0.05, corrected (using the 3dClustSim subroutine of AFNI; (*91*)). Between-group comparisons were performed using a two-sample t-test, modeling individuals as fixed effects and performing cluster correction as described above.

Support vector machine classification analysis with recursive feature elimination

To obtain a model-free confirmation of the effects of pharmacological agents on optogenetic midbrain stimulation, we applied a support vector machine classification analysis with recursive feature elimination (SVM-RFE; (*39*) using scikit-learn (*92*)). Features were defined as activity values in each voxel (within a brain) at each time point during a trial. These analyses allowed us to visualize and verify both where and when BOLD activity reliably discriminated between optogenetic midbrain stimulation versus non-stimulation trials. To find the optimal classification parameters, we first applied support vector machine classifiers with recursive feature elimination (5% per iteration until < 1% were remaining) to volume-masked whole brain data for all acquisitions following stimulation or not (i.e., 26 TRs spanning 13 sec / trial) at varying C-values (representing the robustness of the separation margin between the two classification categories) ranging from .0001 to 1000 by orders of magnitude, and then tested classification performance using "leave one run out" cross-validation. We then visualized which C-value and number of features provided the best classification of optogenetic midbrain stimulation versus non-stimulation trials. Next, we reran the SVM-RFE using these peak classification parameters, and back-projected features that significantly classified midbrain stimulation versus not onto a

four-dimensional representation of brain volumes over time in order to visually verify that predicted features responded to midbrain stimulation or not at the expected time points (Fig. S6). Cross-validation at the optimal C-value and back-projection of peak classification features onto brain volumes were also performed for the pharmacological manipulation datasets and for YFP-control subjects for direct comparison of classification rates. Using the drug-free dataset, SVM-RFE revealed that 2.5% of the features at a classification parameter of C = 1.0 (where C defines the robustness of the separation margin between classification categories) best classified midbrain stimulation versus no stimulation at a peak value of 87% accuracy (cross-validated across runs and subjects). For visual stimulation, 2.5% of the features at a classification parameter of C = 0.001 best classified stimulation versus no stimulation at a peak value of 82% accuracy.

SSFO timeseries correlation analysis (resting state experiments): Preprocessing

Only runs with minimal motion (maximum root mean squared displacement < 0.3 mm) were included in the functional connectivity analysis. Preprocessing for these analyses was as described above, except that temporal filtering employed a bandpass filter spanning 0.005–0.1 Hz, and linear and quadratic trends were removed from the data, in accord with standard protocols for resting state fMRI analysis. Data were pre-whitened to remove autocorrelation. In addition, to control for motion artifacts, we censored high-motion volumes (root mean squared displacement > 0.075 mm), and regressed on 12 motion parameters (roll, pitch, yaw, translation in 3 dimensions, and the first derivative of each of those six parameters). We noted that physiological factors (heart rate, respiratory rate) had minimal impact on BOLD signal fluctuations, therefore we did not include these as regressors in our model.

SSFO timeseries correlation analysis (resting state experiments): brain-wide partial correlation estimation with graphical lasso

Sparse partial correlation matrices were estimated using graphical lasso for each pre-processed dataset (i.e. each run) (*52*). Model selection was performed individually on each graph using the rotation information criterion in the R "huge" package (*53*). To perform a statistical comparison between conditions, we adopted the following screening threshold (motivated by stability selection (*93*)): at least one value in a pairwise relationship must be non-zero in the majority (>

60%) of datasets in either condition. For the pairwise relationships that survived screening, we compared whether they were different under "opsin on" versus "opsin off" conditions by doing an element-wise permutation t-test with 1000 permutations. Results are displayed at an uncorrected threshold of $p < 0.05$.

SSFO timeseries correlation analysis (resting state experiments): seed-based correlation analysis

A seed-based analysis was performed to assess changes in BOLD activity correlations during non-activated and SSFO-activated resting state scans. The seed was a 5-voxel region of interest at the tip of the optical fiber, which was evident in all anatomical and functional volumes and was specified individually for each subject. We extracted the normalized, motion-corrected timeseries for the seed region of interest for each run (averaged across all voxels in the seed), and generated brain-wide functional connectivity maps by calculating the cross-correlation of the seed BOLD activity timeseries with the timeseries for each voxel. The Fisher Z-transformed correlation coefficients for each run were then entered into a group level analysis, where individuals were modeled as fixed effects, and voxel-wise t-tests were used to assess the effect of SSFO activation versus no activation on functional connectivity between the seed region of interest and all brain voxels. For consistency across figures, T-scores were converted to Z-scores and group-level maps were thresholded at $p < 0.05$ after correction for multiple comparisons, as described above.

Correlations between functional imaging data and behavioral parameters

VTA-ChR2 BOLD activity versus self-stimulation behavior

Peak BOLD activity contrast (stimulation on − stimulation off) was obtained from individual scans in manually defined regions of interest (ventral striatum and dorsal striatum), using a standard stereotactic brain atlas as a reference (*94*). The predilection of each subject for the active (self-stimulating) lever in the self-stimulation operant chamber behavioral paradigm was calculated as the ratio of the number of active lever presses to the number of inactive lever presses on the final day of operant chamber training. These values were then entered into a Spearman correlation analysis (using GraphPad Prism software).

SSFO-mediated BOLD activity correlation changes and sucrose preference behavior

A regression analysis was performed to assess the relationship between functional connectivity across the brain during SSFO activation of medial prefrontal cortex and the degree of anhedonia induced in individual subjects. This analysis could, by definition, only include those subjects for whom both sucrose preference behavioral testing and resting state scans had been performed (SSFO subjects: n = 4, YFP subjects: n = 4). The analysis was limited to brain regions showing significantly altered temporal correlations with the medial prefrontal cortex fiber site during SSFO-activated scans versus non-activated scans (Fig. 4i-k). Within this mask, we performed a voxelwise linear regression analysis in which BOLD activity correlation with the medial prefrontal cortex fiber site during light-activated scans was regressed against the subject's sucrose preference on day 3 of sucrose preference testing (the mid-point of the behavioral test), generating a group-level statistical map of brain voxels showing a significant relationship between BOLD activity correlations and behavior across subjects. Fig. 4i-k depicts plots and Pearson correlation coefficients for the relation between these two variables in brain regions showing a significant association with sucrose preference, and for comparison, a brain region (dorsal striatum) which did not show an association with behavior, despite showing a significant change in correlation strength with mPFC during SSFO stimulation.

In vivo electrophysiological experiments

Anesthetized single optrode recordings

To confirm functional expression of SSFO and its response to blue and yellow light pulses, optical stimulation with simultaneous electrophysiological recording using an optrode was performed as described previously (*45*). The optrode consisted of a 1 MΩ tungsten electrode (A-M Systems, Sequim, WA) coupled to a 200 μm 0.37 NA optical fiber (Thorlabs Inc., Newton, NJ). A rat previously injected with AAV5-CKIIα-SSFO-eYFP (> 4 weeks of expression time) was deeply anaesthetized with isoflurane, with body temperature maintained using a heating pad. A midline scalp incision was made and the skin reflected. A 2-3 cm craniotomy was made over the medial prefrontal cortex (AP + 2.7, ML 0.5 (right side)) and the optrode gradually lowered into the medial prefrontal cortex (DV 3-5). Multi-unit recordings were amplified (Model 1800 Microelectrode AC Amplifier, AM Systems), digitized at 30 kHz and bandpass filtered between 0.3-10 kHz and Clampex software (1440A Digidata, Molecular Devices) was used both for

recording the electrical signals as well as controlling light delivery via two diode pumped solid state lasers (OEM Laser systems, Inc., Salt Lake City, UT) (473 nm for SSFO activation and 590 nm for deactivation). Light power was 6 mW at the fiber tip for blue light, and 10 mW at the fiber tip for yellow light.

Awake multi-site electrode array recordings

Freely moving electrophysiological recordings were performed as described previously (*88*). Rats were briefly anesthetized (less than 10 minutes) with isoflurane to allow connection of the headstage (Neuralynx, Bozeman, MT) to the fixed wire array, and rats were allowed to recover for at least one hour prior to the start of recordings. Light power was checked before and after recordings to ensure that the optical fiber was intact. Electrophysiological data was acquired with a 64 channel Digital Lynx data acquisition system. Local field potential (LFP) data was bandpass filtered between 1 Hz and 400 Hz with a sampling frequency of 1550 Hz. Single unit spike data was bandpass filtered between 600 and 6000 Hz and digitized at 32 kHz. During data collection, spiking channels were first referenced to a ground electrode (one electrode in the array chosen for minimal discernible spiking activity). For LFP recordings, the data was subsequently "unreferenced" (ground reference subtracted) during offline analysis. Laser stimulation was controlled using a Master-8 stimulus generator (A.M.P.I. Jerusalem, Israel) and light pulses were recorded simultaneously with the neural data. Recordings were performed in the home cage, in which the rats were free to roam. After a 1 minute baseline recording period, light pulses were delivered in a sequential pattern: a 2 s pulse of continuous 473 nm light (6 mW at fiber tip), followed 28 s later by a 5 s pulse of continuous 590 nm light (10 mW at fiber tip). Higher light power was used for the yellow light in order to maximally ensure inactivation of SSFO. This resulted in a 30 s on / 30 s off stimulation pattern for SSFO which continued for 10 minutes, with a 1 minute "inactive" period at the end of the recording. Prior to sacrifice for histology, 2 of 5 rats were deeply anaesthetized and current was passed through all electrodes to make electrolytic lesions for confirmation of anatomical location.

<u>In vivo electrophysiological data analysis</u>

LFP data analysis

Raw data were initially imported into Neuralynx software (Neuralynx, Inc) for exploratory analysis. Local field potential (LFP) data were subsequently exported to Matlab (Mathworks) for further analysis. Raw traces (unreferenced to ground) were generally not filtered beyond the filtering that was performed during data acquisition (bandpass from 1 Hz to 400 Hz). In two cases, a notch filter centered at 60 Hz was applied to remove power-line noise. A single electrode in each array was chosen at random for LFP analysis. Spectral analysis was performed using Matlab's signal processing toolbox and Chronux (www.chronux.org, (*95*)). Parameters were chosen to allow a frequency resolution of 0.75 Hz and temporal resolution of 500 ms. Coherence plots represent the magnitude of coherence, not phase coherence. Power spectral density plots and coherence versus frequency plots were smoothed using a robust locally weighted regression with a span of 5% (robust loess smoothing, Matlab).

Single unit spiking data analysis

Spikes were imported into Offline Sorter software (Plexon Inc, Dallas, TX) and sorted offline using waveform features (peak and valley heights) and principal components. Spike sorted data was imported into Neuralynx and Matlab software for further analysis. Neural spiking was assessed in the 500 ms preceding and following the first blue light pulse. Channels in which no spikes occurred during this time period were excluded from the analysis.

Histology, imunohistochemistry and confocal imaging

Histological specimens were obtained as described previously (*88*). In brief, rats were deeply anaesthetized with isoflurane and Beuthanasia-D and were transcardially perfused in cold 4% paraformaldehyde perfusion fix solution (Electron Microscopy Services, Hatfield, PA, USA). Brains were extracted and kept in the fixation solution for 24 hours at 4° C and then transferred to 30% sucrose in PBS to equilibrate for 3 days at 4 °C. 40 μm slices were cut on a freezing microtome and stored in cryoprotectant at 4° C. Sections were washed in 1X phosphate buffered saline (Gibco, Life Technologies) then stained with 4',6-diamidino-2-phenylindole (DAPI, 1:50000) for 30 mins, then washed again and mounted on slides with PVA-DAPCO. For staining of midbrain dopamine neurons, sections were washed with PBS and incubated for 60 mins in PBS++ (0.3% Triton-X and 3 % normal donkey serum). Sections were incubated with primary antibody overnight at 4° C. The primary antibody used was chicken anti-tyrosine hydroxylase

(1:500, Aves Labs, Inc., TYH). Sections were then washed in PBS and incubated in secondary antibody conjugated to Alexa Fluor® 647 for three hours at room temperature in PBS++ (1:500, Life Technologies, A-21449). Sections were then washed in PBS and incubated in DAPI for 30 mins, then washed again and mounted on slides with PVA-DAPCO. Confocal imaging of YFP fluorescence (for opsin expression, fiber and electrode placement), antibody staining and DAPI was performed using a Leica TCS SP5 confocal scanning laser microscope with a 5X air objective and 20X, 40X or 63X oil objective.

Sample size calculations

Sample size calculations were performed prior to the start of behavioral experiments, using effect sizes and standard deviations estimated from previous studies and pilot experiments and choosing a desired power of 0.8 and α of 0.05. For example, for optogenetic self-stimulation behavior, previous studies had indicated that the effect was very large, therefore using an estimated effect size between ChR2 expressing subjects versus YFP controls of 1000 lever presses over a 1-2 hour test period, and a standard deviation of 800, the calculated sample size was 6. For sucrose preference, the estimated effect size between SSFO-expressing subjects and YFP controls was a 10% difference in sucrose preference with an estimated standard deviation of 10%, resulting in a calculated sample size of 8 (http://www.statisticalsolutions.net/pss_calc.php).

Rodent demographics for all experiments

Surgeries for virus injections and implants were performed at 8-10 weeks of age.

Experiment (Figures)	**Number of rats**	**Number of scans**	**Age (weeks)**	**Sex**	**Strain**
1) Habituation (Fig. 1a-d)	2	8	24-32	Male	Sprague Dawley
2) fMRI: ChR2 stimulation of dopamine neurons: ChR2 expressing: (Fig. 2c,e,g)	8	34	16-32	Female	Long-Evans, TH-Cre
3) fMRI: ChR2 stimulation of dopamine neurons: YFP expressing: (Fig. 2d,f,h)	4	21	24-32	Female	Long-Evans, TH-Cre
4) Behavior: lever press for dopamine stim ChR2-expressing (Fig. 2i-k, Fig. S3e-h)	8	N/A	12-24	Female	Long-Evans, TH-Cre

5) Behavior: lever press for dopamine stim YFP-expressing (Fig. 2i-k, Fig. S3e-h)	4	N/A	12-24	Female	Long-Evans, TH-Cre
6) fMRI: D1 & D2R antagonism (Fig. 3, Fig. S5, S6)	4	16-18	24-28	Female	Long-Evans, TH-Cre
7) Behavior: eNpHR place preference (Fig. S7b)	6	N/A	16-32	Female	Long-Evans, TH-Cre
8) fMRI: eNpHR inhibition (Fig S7c-h)	6	16-17	28-32	Female	Long-Evans, TH-Cre
9) fMRI: mPFC task-like stimulation SSFO-expressing (Fig. 4d,g, Fig. S9, S10)	6	17	24-32	Male	Sprague Dawley
10) fMRI: mPFC task-like stimulation YFP-expressing (Fig. 4e,h, Fig. S9, S10)	5	20	24-32	Male	Sprague Dawley
11) Behavior: sucrose preference SSFO-expressing (Fig. 4i-k, Fig. S10)	8	N/A	14-16	Male	Sprague Dawley
12) Behavior: sucrose preference YFP-expressing (Fig. 4i-k, Fig. S10)	10	N/A	14-16	Male	Sprague Dawley
13) Behavior: social interaction SSFO-expressing (Fig. 4m,p)	6	N/A	24-26	Male	Sprague Dawley
14) Behavior: social interaction YFP-expressing (Fig. 4m,p)	6	N/A	24-26	Male	Sprague Dawley
15) Behavior: novel object and velocity SSFO-expressing (Fig. 4n,o, Fig. S10)	5	N/A	24-26	Male	Sprague Dawley
16) Behavior: novel object and velocity YFP-expressing (Fig. 4n,o, Fig. S10)	6	N/A	24-26	Male	Sprague Dawley
17) fMRI: dual stimulation (Fig. 5b-f)	6	32 x 2	16-24	Female	Long-Evans, TH-Cre
18) Behavior: dual stimulation (Fig. 5h, Fig. S14)	5-7	N/A	28	Female	Long-Evans, TH-Cre
19) fMRI: mPFC resting state stimulation SSFO-expressing (Fig. 6, Fig. S9, S11, S12)	4	14	24-32	Male	Sprague Dawley
20) fMRI: mPFC resting state stimulation YFP-expressing (Fig. 6, Fig. S9, S11, S12)	4	15	24-32	Male	Sprague Dawley
21) Awake, in vivo electrophysiology: SSFO in mPFC (Fig. S8, S13)	5	N/A	20	Male	Sprague Dawley

The following experiments were performed on the same cohorts:

Dopamine neuron stimulation/inhibition:

Experiment #2,4,6: ChR2-expressing rats: behavior and fMRI

Experiment #3,5: YFP-expressing rats: behavior and fMRI

Experiment #7,8: NpHR-expressing rats: behavior and fMRI

mPFC stimulation:

Experiment #9,11,19: SSFO-expressing rats: behavior and fMRI

Experiment #10,12,20: YFP-expressing rats: behavior and fMRI

Experiment #13,15: SSFO-expressing rats: behavior

Experiment #14,16: YFP-expressing rats: behavior

Dual stimulation:

Experiment #17,18: behavior and fMRI

Supplementary Figures and Figure Legends

Figure S1

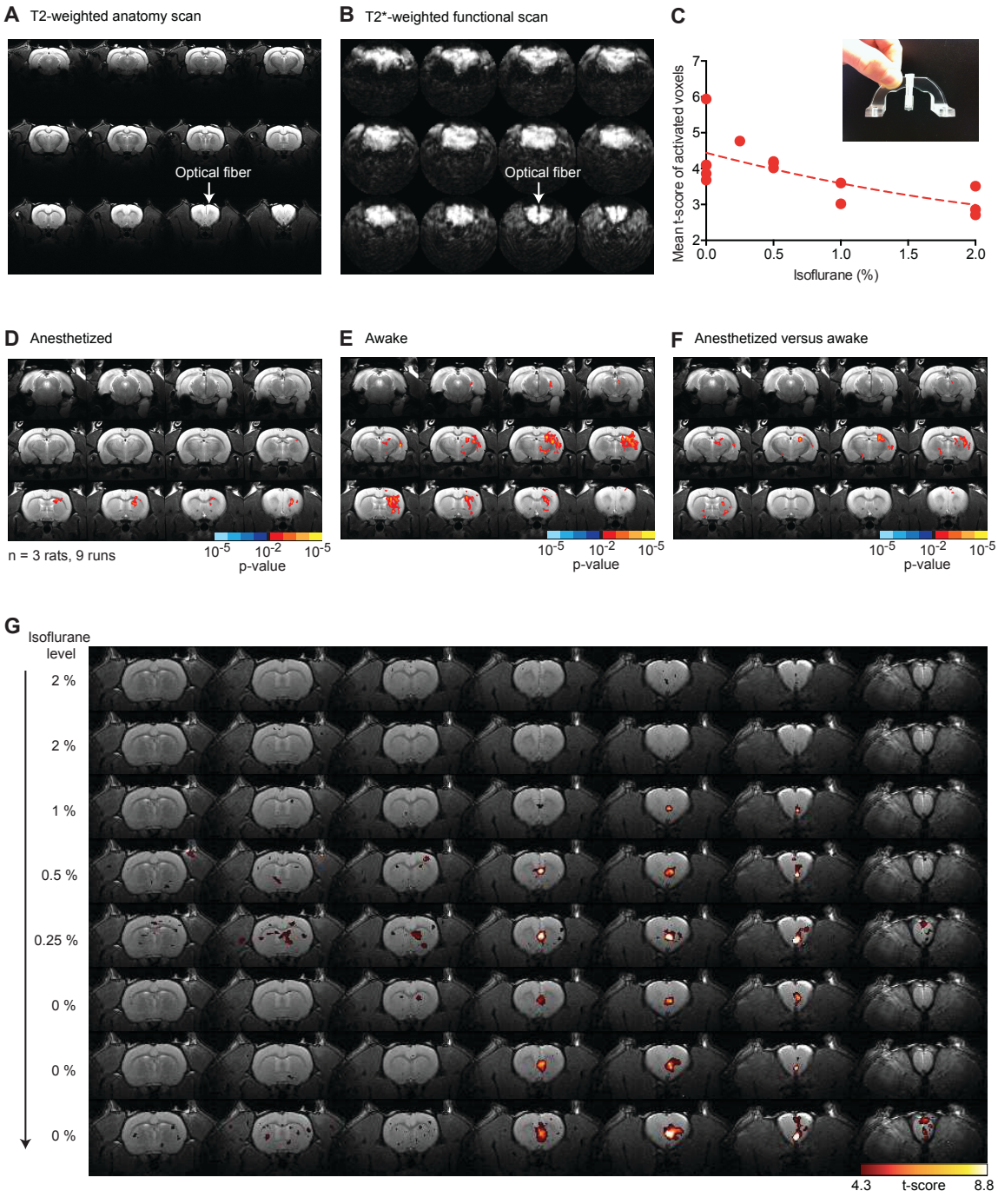
A T2-weighted anatomy scan
Optical fiber
B T2*-weighted functional scan
Optical fiber
C
Mean t-score of activated voxels
7
6
5
4
3
2
0.0
0.5
1.0
1.5
2.0
Isoflurane (%)
D Anesthetized
n = 3 rats, 9 runs
10-5 10-2 10-5
p-value
E Awake
10-5 10-2 10-5
p-value
F Anesthetized versus awake
10-5 10-2 10-5
p-value
G
Isoflurane level
2 %
2 %
1 %
0.5 %
0.25 %
0 %
0 %
0 %
4.3
t-score
8.8

Fig. S1

Awake optogenetic functional MRI

A, Example of T2-weighted anatomy scan. **B**, Example of T2*-weighted, single-shot spiral in-out gradient echo functional scan, 30 mm field of view, 0.47 mm x 0.47mm in-plane spatial resolution, 1 mm slice thickness, 15 slices, TR/TE 500/15 ms, single-channel 2.5cm surface coil. **C**, Mean t-score for activated voxels ($p < 0.01$) vs. anesthesia level. Data is from 1 rat, 2 scanning sessions, 1 month apart. Inset: MRI-compatible Perspex head post and attachment for MRI cradle. **D-F**: Comparison of BOLD activity during the anesthetized versus awake state during optogenetic stimulation of midbrain dopamine neurons (ChR2 stimulation as described in Fig 2). Z-score maps for evoked BOLD activity to ChR2 stimulation are shown for 3 rats while anesthetized (inhaled isoflurane $\geq 0.5\%$) (9 runs) **(D**) and while awake (inhaled isoflurane = 0%) (9 runs) (**E**) and the statistical comparison between the two conditions (**F**). The anesthetized and awake conditions were matched for subject, as scans were collected during the same scanning sessions for each of the 3 rats, with isoflurane level titrated down from 2% to 0%. Display threshold was set at $p < 0.05$ (corrected for multiple comparisons using a minimum cluster-size threshold ($K > 5$ functional voxels [80 transformed voxels], uncorrected p-value < 0.01). Gradations in color (e.g. red-orange-yellow) indicate incremental p-value thresholds of one order of magnitude. **G**, 8 sequential t-score maps of BOLD response to SSFO stimulation in mPFC in a single subject as isoflurane level was titrated from 2% to 0% (display threshold is for an uncorrected p-value < 0.0001).

Figure S2

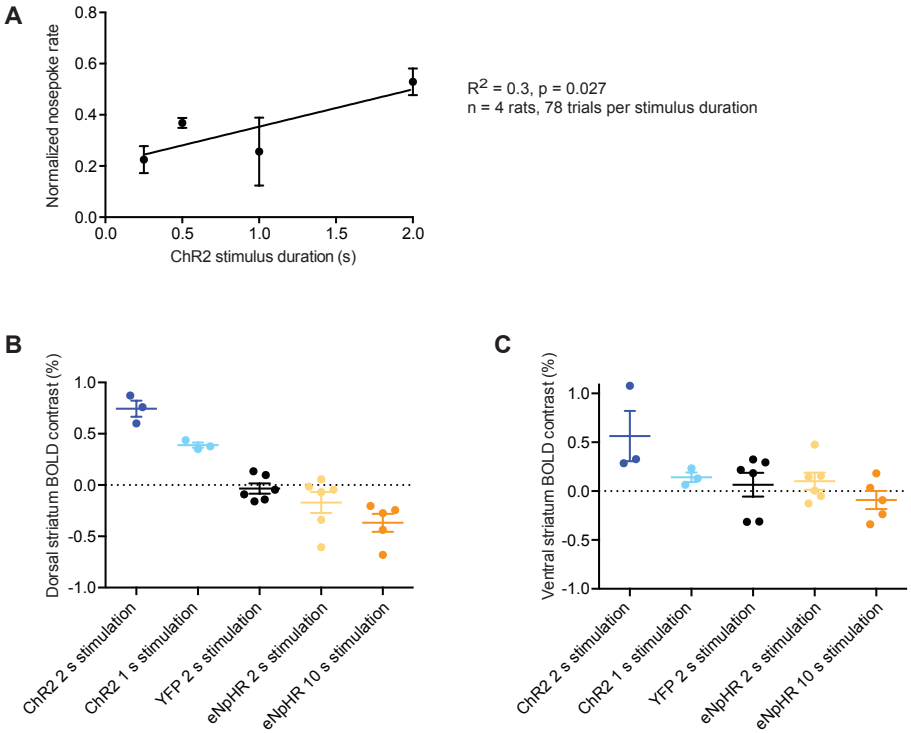
A
Normalized nosepoke rate
0.0
0.2
0.4
0.6
0.8
0.0
0.5
1.0
1.5
2.0
ChR2 stimulus duration (s)
R2 = 0.3, p = 0.027
n = 4 rats, 78 trials per stimulus duration
B
Dorsal striatum BOLD contrast (%)
1.0
0.5
0.0
-0.5
-1.0
ChR2 2 s stimulation
ChR2 1 s stimulation
YFP 2 s stimulation
eNpHR 2 s stimulation
eNpHR 10 s stimulation
C
Ventral striatum BOLD contrast (%)
1.0
0.5
0.0
-0.5
-1.0
ChR2 2 s stimulation
ChR2 1 s stimulation
YFP 2 s stimulation
eNpHR 2 s stimulation
eNpHR 10 s stimulation

Fig. S2

Dose response to burst stimulation duration

A, TH-cre transgenic rats were trained to nose-poke for optogenetic ChR2 stimulation of their midbrain dopamine neurons across different light stimulus durations (0.25 s to 2 s). Within each stimulus, light pulses were delivered at 20 Hz (10 ms pulse width). There was a significant positive linear relationship between normalized nose-poke rate (normalized to each rat's individual maximum) and stimulus duration ($R^2 = 0.3$, $p = 0.027$ for slope significantly different to 0, n = 4 rats, 78 trials, data pooled across two consecutive testing days). **B**, Dorsal striatum and **C**, ventral striatum BOLD contrast for ChR2-expressing rats in response to 1 s and 2 s stimulus duration (470 nm, 20 Hz, 10 ms pulse width, n = 1 rat, 3 runs per stimulus duration), YFP-control rats in response to 2 s stimulus duration (470 nm, 20 Hz, 10 ms pulse width, n = 3 rats, 6 runs) and eNpHR3.0-expressing rats in response to 2 s and 10 s stimulus duration (590 nm, continuous light, n = 2 rats, 5-6 runs per stimulus duration).

Figure S3

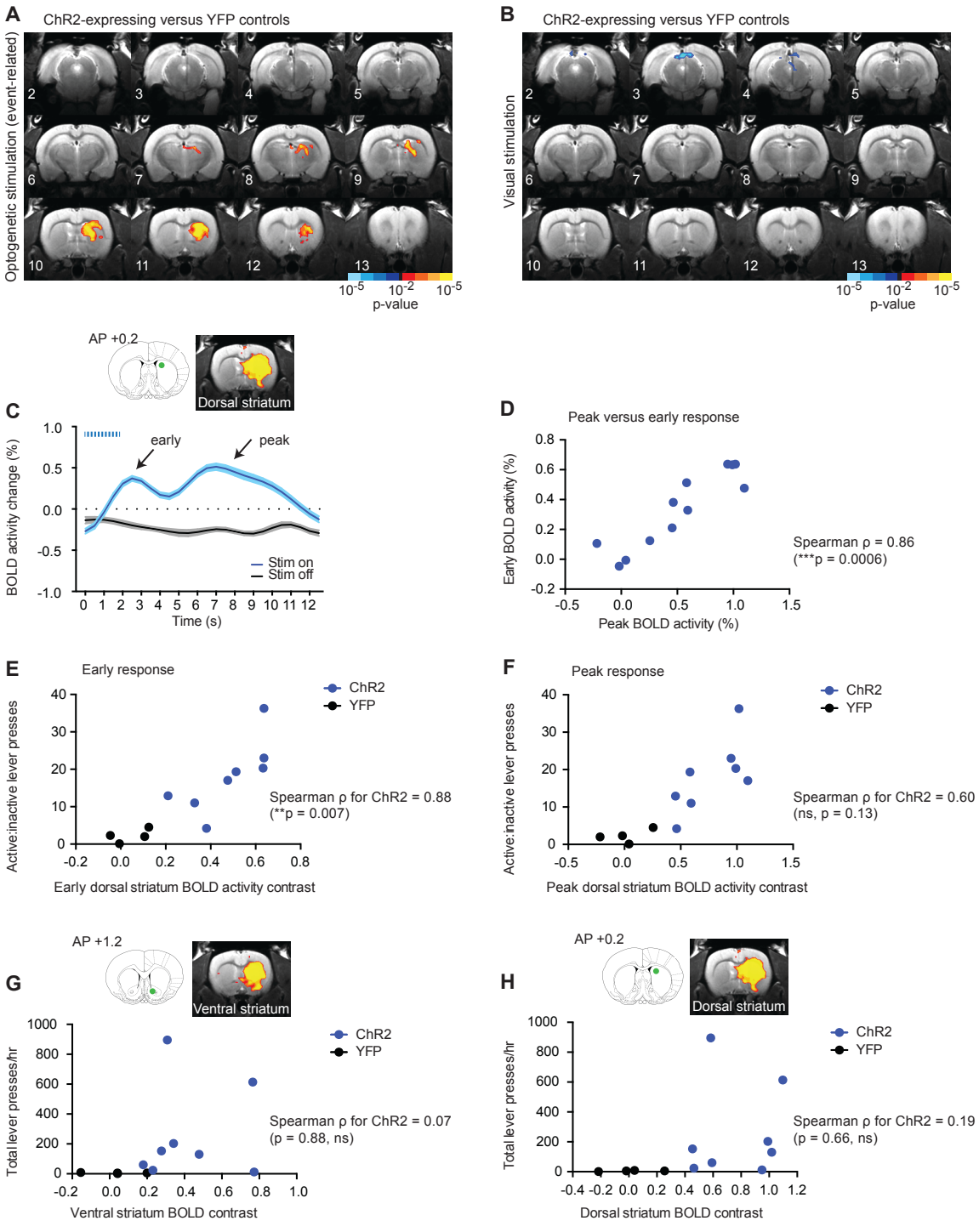
A
ChR2-expressing versus YFP controls
Optogenetic stimulation (event-related)
2
3
4
5
6
7
8
9
10
11
12
13
10-5
10-2
10-5
p-value
B
ChR2-expressing versus YFP controls
Visual stimulation
p-value
AP +0.2
Dorsal striatum
C
BOLD activity change (%)
early
peak
Stim on
Stim off
Time (s)
D
Peak versus early response
Early BOLD activity (%)
Peak BOLD activity (%)
Spearman ρ = 0.86
(***p = 0.0006)
E
Early response
ChR2
YFP
Active:inactive lever presses
Spearman ρ for ChR2 = 0.88
(**p = 0.007)
Early dorsal striatum BOLD activity contrast
F
Peak response
ChR2
YFP
Active:inactive lever presses
Spearman ρ for ChR2 = 0.60
(ns, p = 0.13)
Peak dorsal striatum BOLD activity contrast
AP +1.2
Ventral striatum
G
Total lever presses/hr
ChR2
YFP
Spearman ρ for ChR2 = 0.07
(p = 0.88, ns)
Ventral striatum BOLD contrast
AP +0.2
Dorsal striatum
H
Total lever presses/hr
ChR2
YFP
Spearman ρ for ChR2 = 0.19
(p = 0.66, ns)
Dorsal striatum BOLD contrast

Fig. S3

Striatal BOLD activity and relationship to behavior

A,**B**, Z-score map of between-group comparison for ChR2-expressing versus YFP-control groups for optogenetic dopaminergic midbrain stimulation (**A**) and visual stimulation (**B**). For ChR2 group: n = 8 rats, 34 runs, for YFP-control group, n = 4 rats, 21 runs. Display threshold was set at $p < 0.05$, corrected for multiple comparisons using a minimum cluster-size threshold ($K > 5$ functional voxels [80 transformed voxels], uncorrected p-value < 0.01). Gradations in color (e.g. red-orange-yellow) indicate incremental p-value thresholds of one order of magnitude. **C**, Illustration of "early" versus "peak" BOLD activity in the dorsal striatum to ChR2 stimulation of midbrain dopaminergic neurons. **D**, Relationship between the early (2-3 s) response and peak (6-7 s) BOLD activity contrast in the dorsal striatum. Spearman $\rho = 0.86$, $p = 0.0006$. **E**, There was a positive correlation between active lever preference (active to inactive lever press ratio during operant chamber self-stimulation behavioral testing) and the early (2-3 s) dorsal striatum "inflow-related" response for ChR2 subjections (Spearman $\rho = 0.88$, $p = 0.007$, $n = 8$). The early response likely represents vascular inflow to the region, enhancing signal independently of blood oxygenation level (*33*). **F**, There was not a significant correlation between the active to inactive lever press ratio and peak dorsal striatum BOLD activity contrast for ChR2-expressing (n = 8) and YFP-control (n = 4) subjects. Spearman ρ for ChR2-subjects = 0.595 ($p = 0.13$). **G,H**, Relationship between total number of lever presses (active + inactive) and BOLD activity contrast in the ventral striatum (**G**) and dorsal striatum (**H**) for ChR2-expressing (n = 8) and YFP-control (n = 4) subjects. Spearman ρ for ChR2-subjects in ventral striatum = 0.071 ($p = 0.88$), and dorsal striatum = 0.191 ($p = 0.66$).

Figure S4

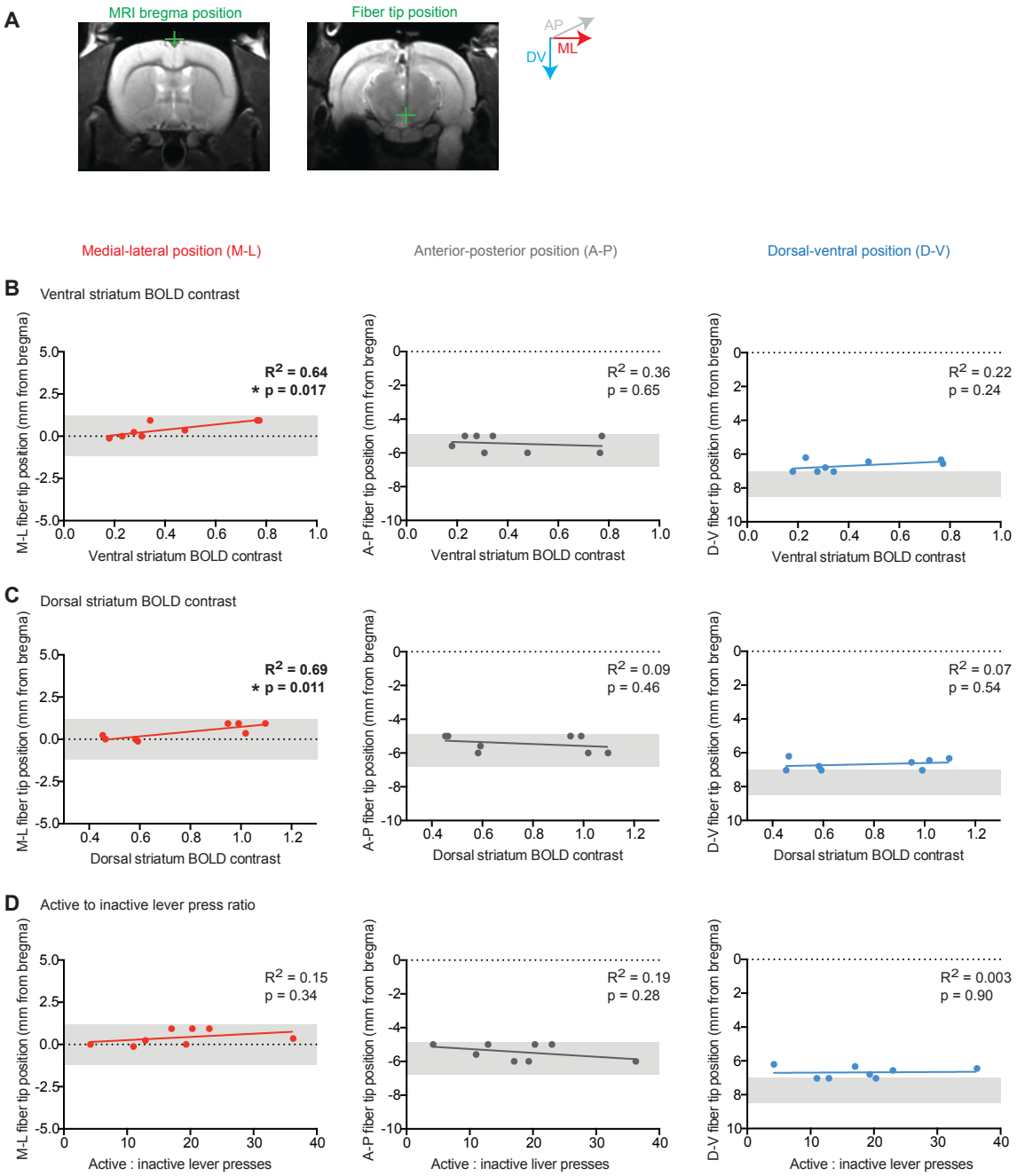
A
MRI bregma position
Fiber tip position
AP
ML
DV
Medial-lateral position (M-L)
Anterior-posterior position (A-P)
Dorsal-ventral position (D-V)
B
Ventral striatum BOLD contrast
M-L fiber tip position (mm from bregma)
R2 = 0.64
* p = 0.017
Ventral striatum BOLD contrast
A-P fiber tip position (mm from bregma)
R2 = 0.36
p = 0.65
Ventral striatum BOLD contrast
D-V fiber tip position (mm from bregma)
R2 = 0.22
p = 0.24
Ventral striatum BOLD contrast
C
Dorsal striatum BOLD contrast
M-L fiber tip position (mm from bregma)
R2 = 0.69
* p = 0.011
Dorsal striatum BOLD contrast
A-P fiber tip position (mm from bregma)
R2 = 0.09
p = 0.46
Dorsal striatum BOLD contrast
D-V fiber tip position (mm from bregma)
R2 = 0.07
p = 0.54
Dorsal striatum BOLD contrast
D
Active to inactive lever press ratio
M-L fiber tip position (mm from bregma)
R2 = 0.15
p = 0.34
Active : inactive lever presses
A-P fiber tip position (mm from bregma)
R2 = 0.19
p = 0.28
Active : inactive liver presses
D-V fiber tip position (mm from bregma)
R2 = 0.003
p = 0.90
Active : inactive lever presses

Fig. S4

Striatal BOLD activity and relationship to fiber tip position

A, Definition of "bregma" on individual rat MRI scan and calculation of fiber tip position relative to the MRI-defined bregma. The MRI-defined bregma was located as close as possible to the anatomical position defined as bregma in the Paxinos and Watson Stereotactic Rat Brain Atlas. Fiber tip position was defined in the three standard stereotactic dimensions relative to bregma: dorsal-ventral (D-V), medial-lateral (M-L), anterior-posterior (A-P). In the plots below the grey shaded regions indicate the spatial extent of the rat ventral tegmental area (VTA) in each dimension. In the D-V dimension the fiber tip was intentionally positioned above the VTA (dorsal surface), to avoid penetration and damage of the VTA by the optical fiber. **B**, Relationship between fiber tip position in three dimensions and ventral striatal BOLD contrast across individual rats. A significant linear correlation was observed for the M-L location of the fiber tip, $R^2 = 0.64$, $p = 0.017$ for slope significantly different to 0, $n = 8$ rats. No significant correlation was seen for the other anatomical dimensions. **C**, Relationship between fiber tip position in three dimensions and dorsal striatal BOLD contrast across individual rats. A significant linear correlation was observed for the M-L location of the fiber tip, $R^2 = 0.649$, $p = 0.0171$ for slope significantly different to 0, $n = 8$ rats. No significant correlation was seen for the other anatomical dimensions. **D**, Relationship between fiber tip position in three dimensions and self-stimulation behavior (defined as ratio of active lever to inactive lever presses) across individual rats. No significant correlation was seen in any dimension.

Figure S5

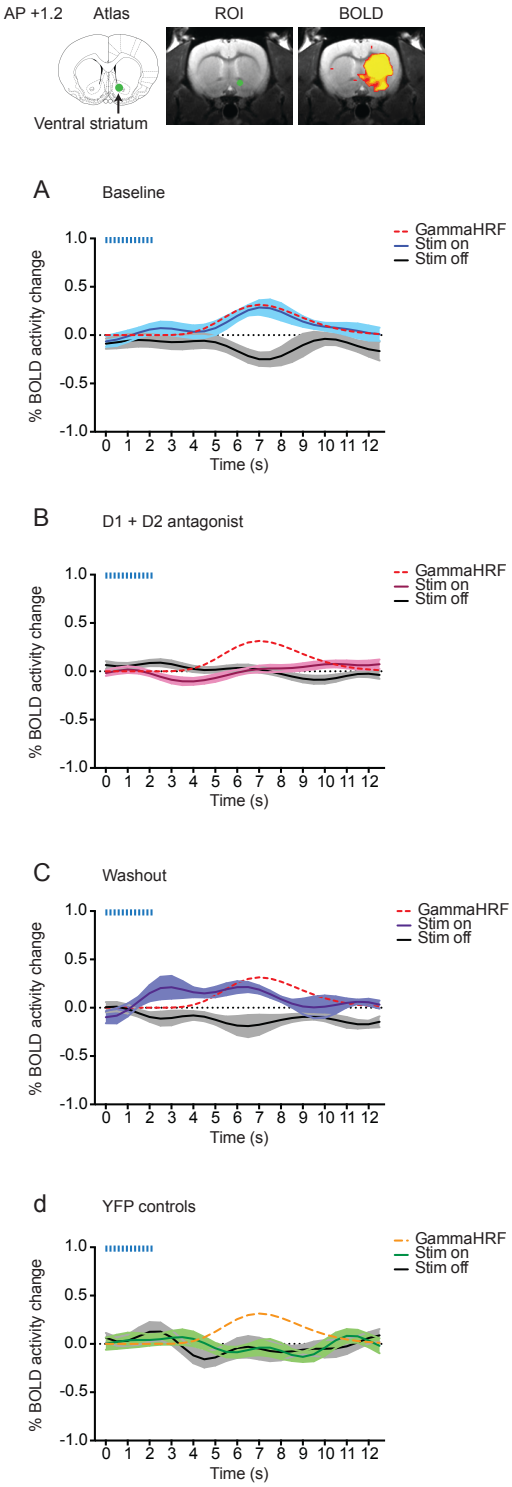
AP +1.2
Atlas
ROI
BOLD
Ventral striatum
A
Baseline
B
D1 + D2 antagonist
C
Washout
d
YFP controls
GammaHRF
Stim on
Stim off
% BOLD activity change
1.0
0.5
0.0
-0.5
-1.0
0 1 2 3 4 5 6 7 8 9 10 11 12
Time (s)

Fig. S5

Average BOLD activity time courses in response to ChR2 stimulation of midbrain dopamine neurons in ventral striatum under different experimental conditions, with gamma variate function superimposed.

Timing of light delivery is indicated above the plots by dashed blue line. Location of regions of interest (ROIs) containing voxels used for time course extraction is indicated by the images above plots. Mean (solid line) and SEM (shaded region, where n = number of runs) are shown for **A**, baseline condition (n = 4 rats, 16 runs), **B**, during administration of D1 and D2 receptor antagonists (n = 4 rats, 22 runs) and **C**, for YFP-control subjects (n = 4 rats, 16 runs, YFP data also shown in Figure 2h). A commonly used "human-like" gamma variate hemodynamic response function (HRF) is overlaid on the plots for comparison (red dashed line).

Figure S6

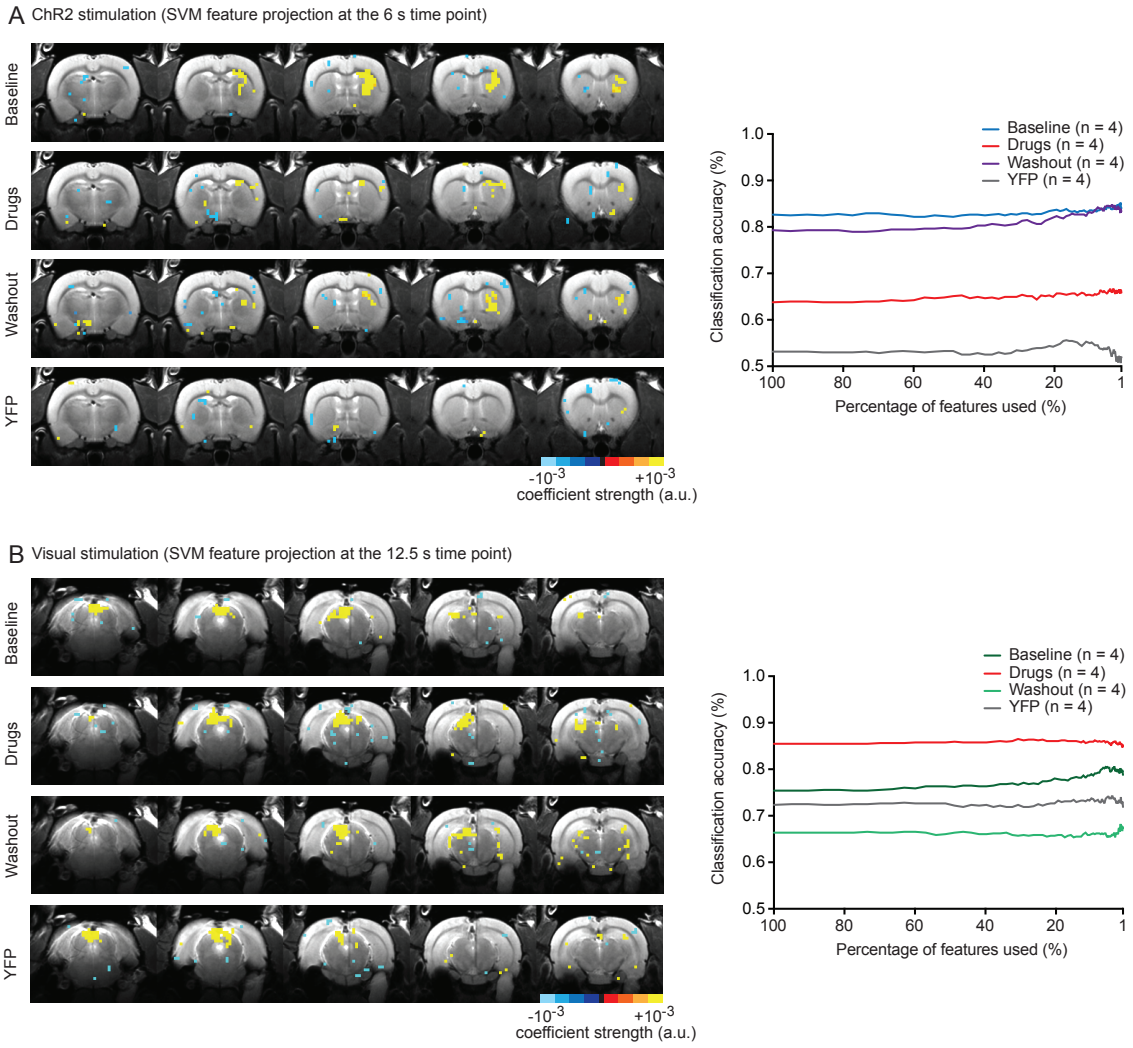
A ChR2 stimulation (SVM feature projection at the 6 s time point)
Baseline
Drugs
Washout
YFP
-10-3
+10-3
coefficient strength (a.u.)
Baseline (n = 4)
Drugs (n = 4)
Washout (n = 4)
YFP (n = 4)
Classification accuracy (%)
1.0
0.9
0.8
0.7
0.6
0.5
100
80
60
40
20
1
Percentage of features used (%)
B Visual stimulation (SVM feature projection at the 12.5 s time point)
Baseline
Drugs
Washout
YFP
-10-3
+10-3
coefficient strength (a.u.)
Baseline (n = 4)
Drugs (n = 4)
Washout (n = 4)
YFP (n = 4)
Classification accuracy (%)
1.0
0.9
0.8
0.7
0.6
0.5
100
80
60
40
20
1
Percentage of features used (%)

Fig. S6

Results of a model-free multivariate classification analysis using support vector machine learning with recursive feature elimination (SVM with RFE)

A, Brain maps show features (voxels at each point in time) able to classify (using 'leave-one-run-out' cross-validation) whether ChR2 stimulation had occurred or not during a trial. Results are overlaid on selected brain slices (with focus on striatum) confirming the peak in activity seen in the previous ROI-based time course analyses at 6-7 s post stimulation (Fig. 3). SVM with RFE analysis was performed for the pharmacological dataset (baseline, D1 and D2 antagonists and washout) and for YFP-controls, revealing much poorer classification accuracies during the drug administration condition and for YFP-control subjects than during baseline or washout conditions. **B**, For visual stimulation, classification rates were greater than 70% in all conditions, and were greatest (86%) during D1 and D2 receptor antagonist administration.

Figure S7

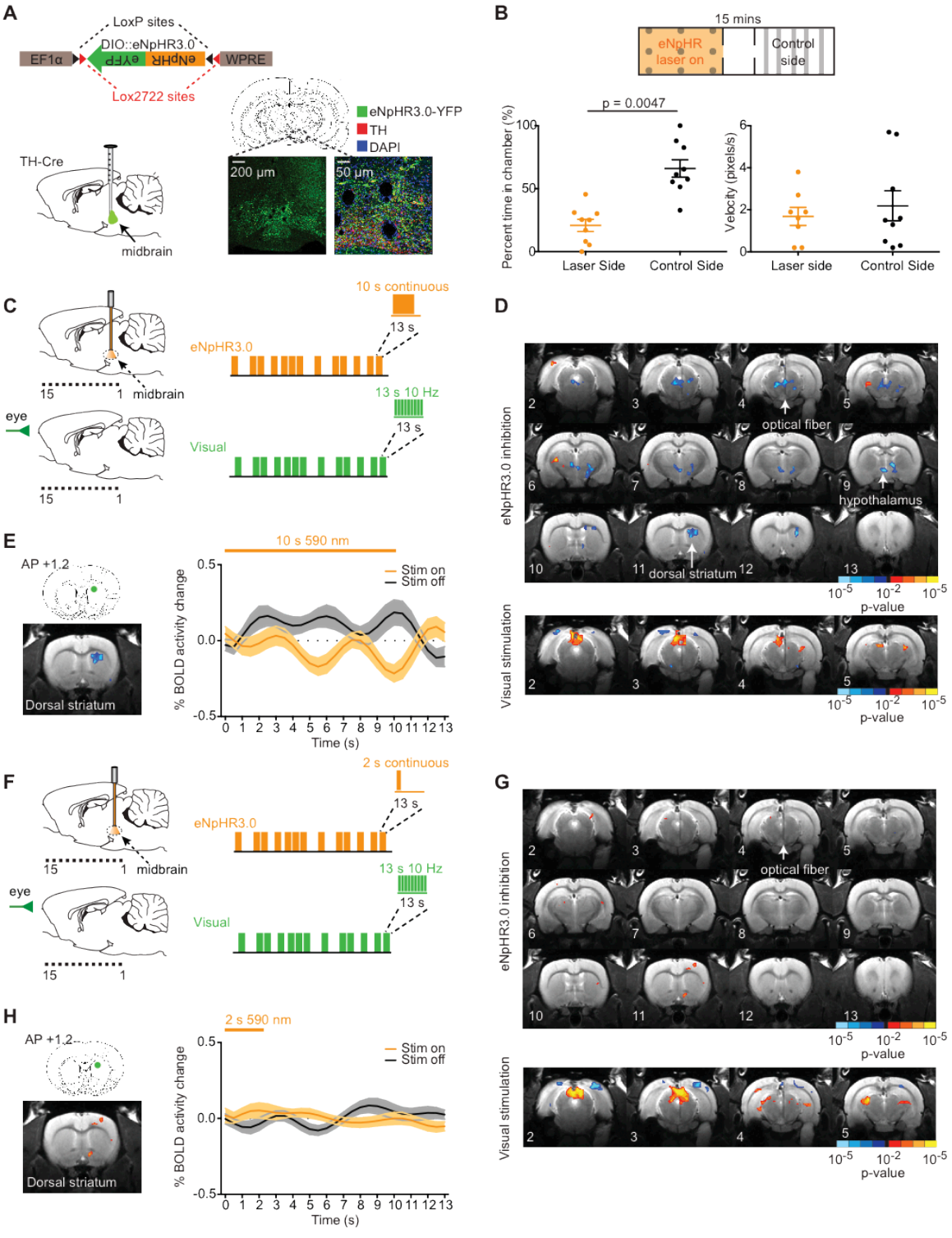
A
LoxP sites
DIO::eNpHR3.0
EF1α
eNpHR
eYFP
WPRE
Lox2722 sites
eNpHR3.0-YFP
TH
DAPI
TH-Cre
midbrain
200 μm
50 μm
B
15 mins
eNpHR laser on
Control side
p = 0.0047
Percent time in chamber (%)
Laser Side
Control Side
Velocity (pixels/s)
Laser side
Control Side
C
10 s continuous
13 s
eNpHR3.0
13 s 10 Hz
13 s
Visual
eye
midbrain
D
eNpHR3.0 inhibition
optical fiber
hypothalamus
dorsal striatum
p-value
Visual stimulation
E
AP +1.2
Dorsal striatum
10 s 590 nm
Stim on
Stim off
% BOLD activity change
Time (s)
F
2 s continuous
13 s
eNpHR3.0
13 s 10 Hz
13 s
Visual
eye
midbrain
G
eNpHR3.0 inhibition
optical fiber
p-value
Visual stimulation
H
AP +1.2
Dorsal striatum
2 s 590 nm
Stim on
Stim off
% BOLD activity change
Time (s)

Fig. S7

Optogenetic inhibition of midbrain dopaminergic neurons

A, Schematic of Cre-dependent eNpHR3.0 construct and sagittal view of injection site in the midbrain. Confocal images demonstrating eNpHR3.0 expression in dopaminergic neurons in the midbrain. Green: eNpHR3.0-YFP, red: tyrosine hydroxylase, blue: DAPI. **B**, Real time place preference was assessed for 15 mins, during which time rats were allowed to freely roam between 3 chambers: a chamber in which yellow light was delivered to midbrain dopamine neurons, a small central chamber and a control chamber where no stimulation was given. Left panel: Mild real time place aversion was seen to eNpHR3.0 inhibition of the dopaminergic midbrain (paired two-tailed t-test $p = 0.0047$, $t = 3.870$, $df = 8$, number of pairs = 9). Right panel: velocity of locomotion during real-time place preference test with eNpHR3.0 inhibition of midbrain dopamine neurons. Velocity was slightly but not significantly lower on the side of eNpHR3.0 inhibition (paired two-tailed t-test $p = 0.4216$, $t = 0.8536$, $df = 7$, number of pairs = 8). **C**, Schematic of event-related design for eNpHR3.0-mediated inhibition in midbrain: 16 pseudorandom stimulation epochs consisting of 10 s continuous light pulses (590 nm, ~6-7 mW). with at least 11 s recovery time between bursts. For visual stimulation: 16 pseudorandom stimulation epochs consisting of 13 s 10 Hz (20 ms pulse width) green light flashes in front of the eye. **D**, Z-score map of BOLD activity changes in response to 10 s eNpHR3.0 stimulation of midbrain dopamine neurons and visual stimulation (n = 6 rats, 16 runs). Display threshold was set at $p < 0.05$, corrected for multiple comparisons using a minimum cluster-size threshold ($K >$ 5 functional voxels [80 transformed voxels], uncorrected p-value < 0.01), Gradations in color (e.g. navy-blue-cyan) indicate incremental p-value thresholds of one order of magnitude. **E**, Average stimulation-locked BOLD activity time course in the dorsal striatum in response to 10 s inhibition of dopamine neurons in the midbrain by eNpHR3.0 (n = 6 rats, 16 runs, shaded region is SEM where n = number of runs). **F**, Short duration inhibition of midbrain dopaminergic neurons with 2 s light pulses. **G**, Z-score map of BOLD activity changes in response to 2 s eNpHR3.0 stimulation of midbrain dopamine neurons and visual stimulation (n = 5 rats, 17 runs). **H**, Average stimulation-locked BOLD activity time course in the dorsal striatum in response to 2 s inhibition of dopamine neurons in the midbrain by eNpHR3.0 (n = 5 rats, 17 runs, shaded region is SEM where n = number of runs).

Figure S8

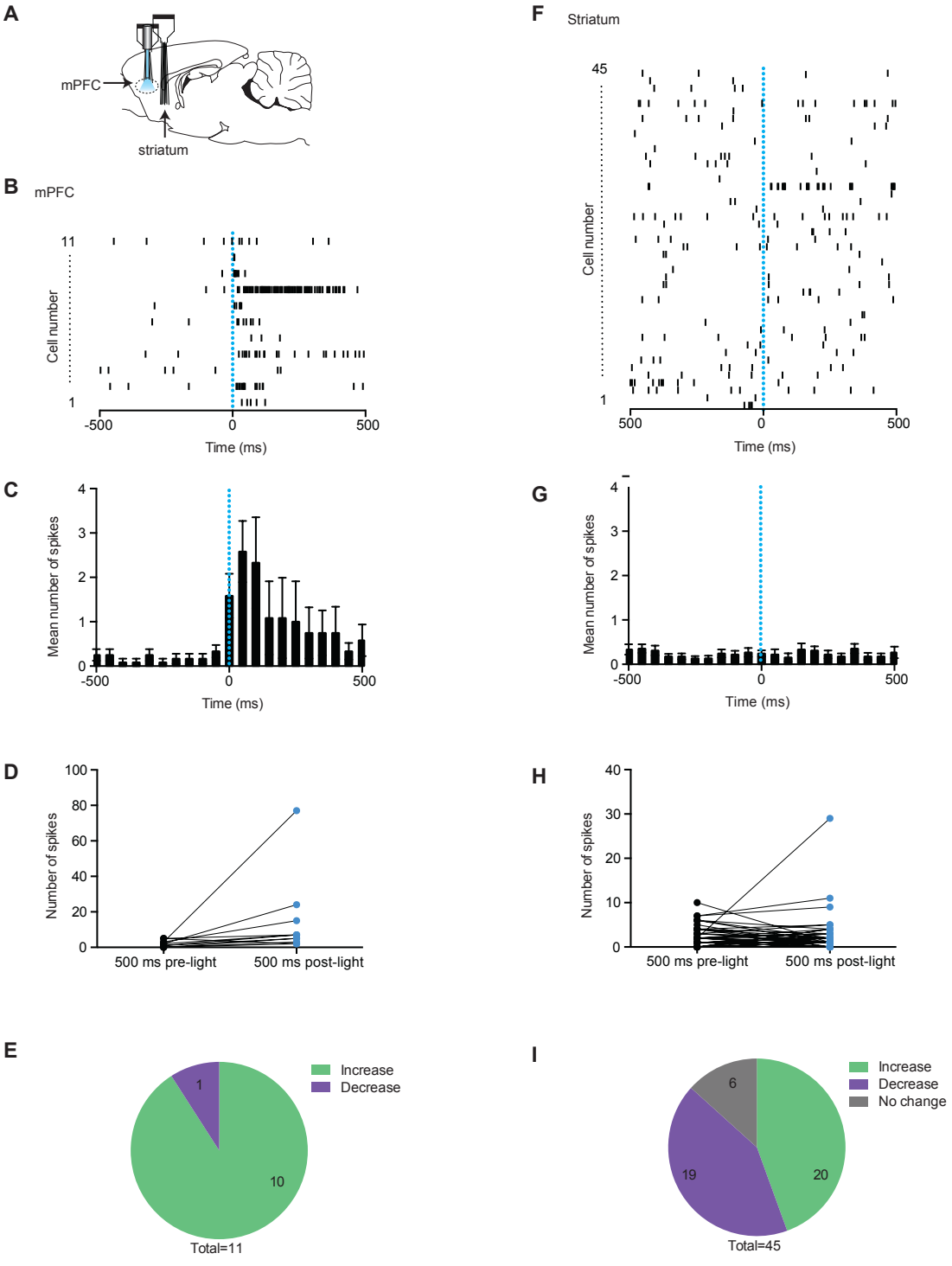
A
mPFC
striatum
B
mPFC
11
Cell number
1
-500
0
500
Time (ms)
C
Mean number of spikes
4
3
2
1
0
-500
0
500
Time (ms)
D
Number of spikes
100
80
60
40
20
0
500 ms pre-light
500 ms post-light
E
Increase
Decrease
1
10
Total=11
F
Striatum
45
Cell number
1
500
0
500
Time (ms)
G
Mean number of spikes
4
3
2
1
0
-500
0
500
Time (ms)
H
Number of spikes
40
30
20
10
0
500 ms pre-light
500 ms post-light
I
Increase
Decrease
No change
6
19
20
Total=45

Fig. S8

In vivo awake single spike recordings in mPFC and striatum

A, Schematic of dual stimulation electrophysiological recording sites in mPFC and ventral striatum with fixed multi-electrode arrays, with an optical fiber included at the mPFC recording site. Data is shown for all active neurons at both locations. Active neurons were defined as those exhibiting at least one spike during 1 s surrounding the first blue light pulse. **B**, Raster plot of spike timing for all spikes for all active mPFC recorded neurons relative to the first blue light pulse. The vertical blue dashed line indicates the timing of the first blue pulse. Each horizontal line represents 1 neuron, each black tick represents one action potential. **C**, Mean peri-stimulus time histogram for all active mPFC neurons (error bars indicated SEM across all 11 neurons), bin size is 50 ms. The vertical blue dashed line indicates the timing of the first blue pulse. **D**, Change in number of spikes between the 500 ms preceding and following the first blue light pulse. Each black (pre) and blue (post) data point pair and connecting line represents an individual mPFC neuron. **E**, Summary pie chart of firing changes for all active mPFC neurons: 10/11 neurons showed an increase in firing in the 500 ms following the blue light pulse compared to the preceding 500 ms and 1 neuron showed a decrease in firing. **F**, Raster plot of spike timing for all spikes for all active striatal recorded neurons relative to the first blue light pulse. The vertical blue dashed line indicates the timing of the first blue pulse. Each horizontal line represents 1 neuron, each black tick represents one action potential. **G**, Mean peri-stimulus time histogram for all active striatal neurons (error bars indicated SEM across all 45 neurons), bin size is 50 ms. The vertical blue dashed line indicates the timing of the first blue pulse. **H**, Change in number of spikes between the 500 ms preceding and following the first blue light pulse. Each black (pre) and blue (post) data point pair and connecting line represents an individual striatal neuron. **I**, Summary pie chart of firing changes for all active striatal neurons: 20/45 neurons showed an increase in firing in the 500 ms following the blue light pulse compared to the preceding 500 ms, 19/45 neurons showed a decrease in firing and 6 neurons showed no change in firing.

Figure S9

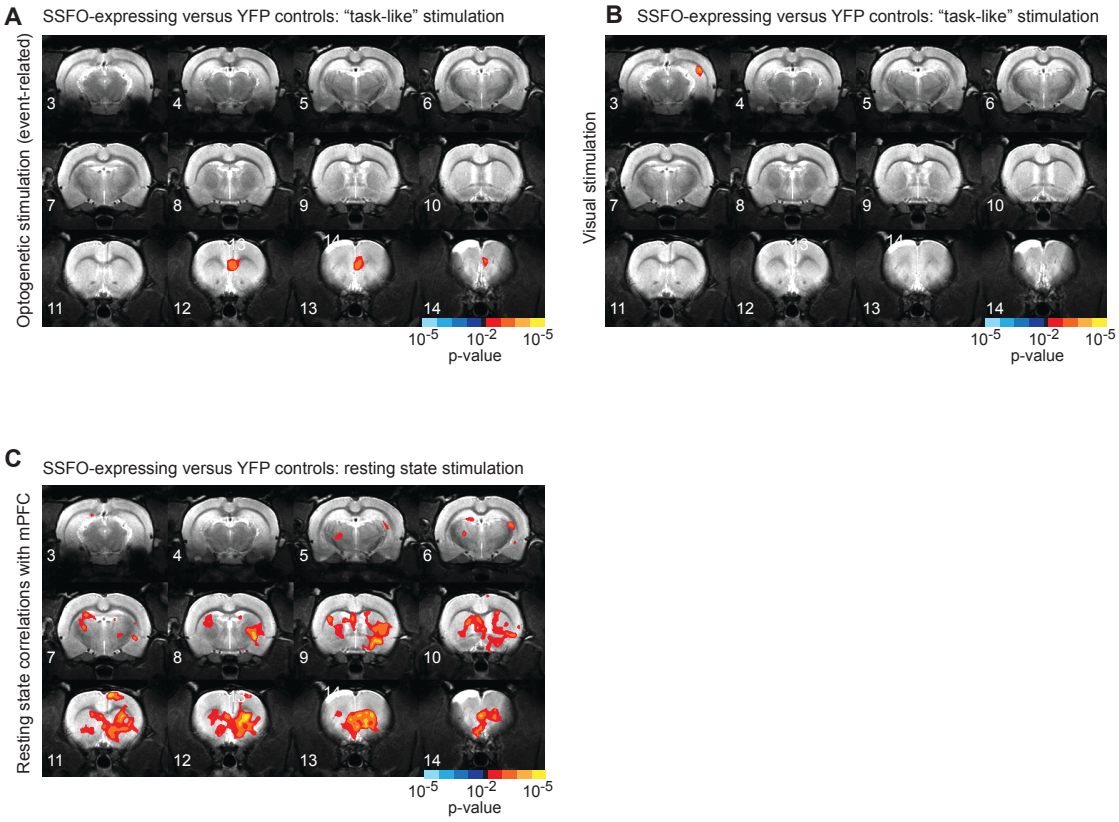
A
SSFO-expressing versus YFP controls: “task-like” stimulation
Optogenetic stimulation (event-related)
3
4
5
6
7
8
9
10
11
12
13
14
10-5
10-2
10-5
p-value
B
SSFO-expressing versus YFP controls: “task-like” stimulation
Visual stimulation
3
4
5
6
7
8
9
10
11
12
13
14
10-5
10-2
10-5
p-value
C
SSFO-expressing versus YFP controls: resting state stimulation
Resting state correlations with mPFC
3
4
5
6
7
8
9
10
11
12
13
14
10-5
10-2
10-5
p-value

Fig. S9

Between-group statistical comparisons for SSFO versus YFP ofMRI experiments: event-related and resting state

A-**C**, Z-score maps of between-group comparisons for SSFO-expressing subjects versus YFP-controls for **A**, event-related optogenetic stimulation of mPFC with SSFO **B**, visual stimulation and **C,** optogenetic modulation of resting state BOLD activity correlations seeded from the mPFC. For event-related stimulation, SSFO group: n = 6 rats, 17 runs, YFP-control group, n = 5 rats, 20 runs. For resting state stimulation: SSFO group: n = 4 rats, 14 runs, YFP-control group: n = 4 rats, 15 runs. Display threshold was set at $p < 0.05$, corrected for multiple comparisons using a minimum cluster-size threshold ($K > 5$ functional voxels [80 transformed voxels], uncorrected p-value < 0.01). Gradations in color (e.g. red-orange-yellow) indicate incremental p-value thresholds of one order of magnitude.

Figure S10

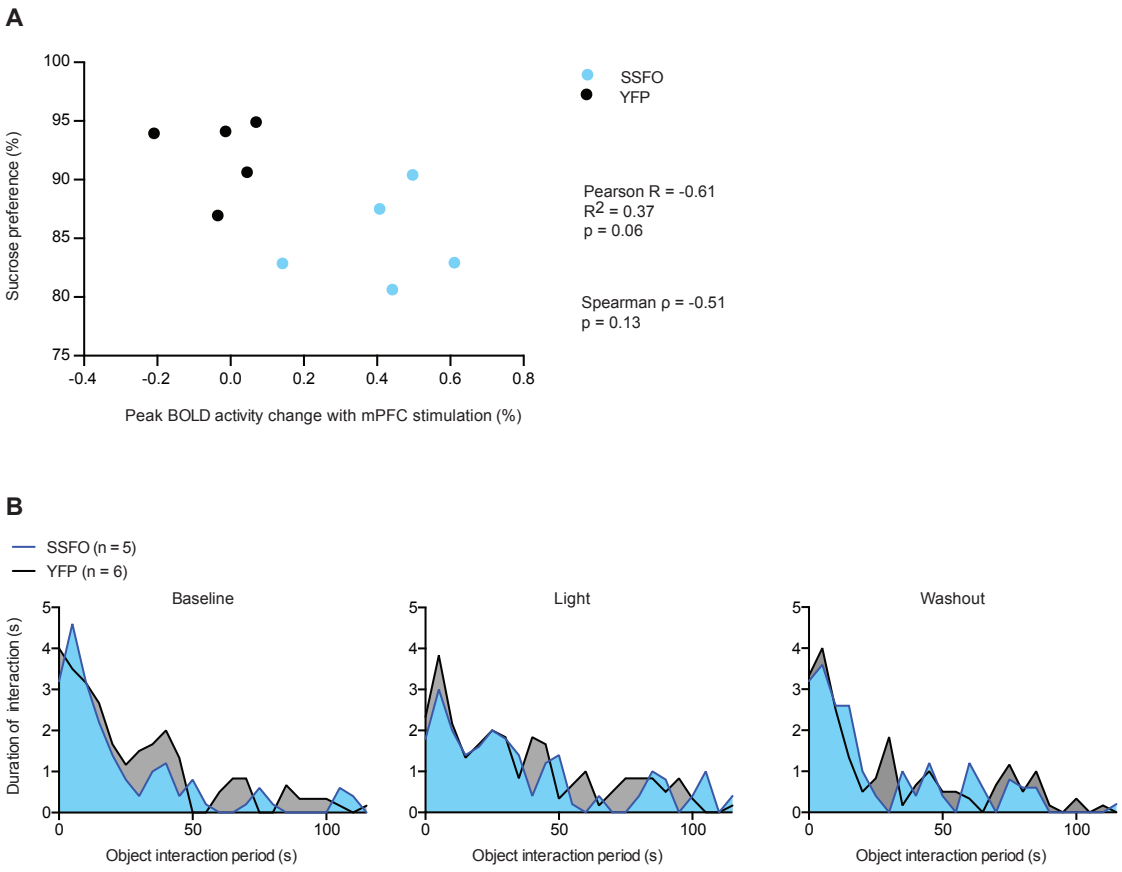
A
100
95
90
85
80
75
Sucrose preference (%)
-0.4
-0.2
0.0
0.2
0.4
0.6
0.8
Peak BOLD activity change with mPFC stimulation (%)
SSFO
YFP
Pearson R = -0.61
R2 = 0.37
p = 0.06
Spearman ρ = -0.51
p = 0.13
B
SSFO (n = 5)
YFP (n = 6)
Baseline
Light
Washout
Duration of interaction (s)
Object interaction period (s)
Object interaction period (s)
Object interaction period (s)

Fig. S10

Cortical modulation of natural reward-seeking behavior: additional analyses

A, Relationship between peak BOLD activity in mPFC during SSFO (or YFP-control) event-related stimulation in MRI scanner and sucrose preference on day 3 of light stimulation in the sucrose preference test. Results for individual rats are shown (n = 5 for SSFO and YFP-expressing subjects. Parametric and non-parametric correlations were performed across both groups: Pearson R = -0.61, R^2 = 0.37, p = 0.06, Spearman ρ = -0.51, p = 0.13. **B**, Interaction with a novel object over time. Average time course of interaction with a novel object over the duration of the interaction period, at baseline, following mPFC light stimulation, and after a washout period (n = 5 for SSFO, n = 6 for YFP).

Figure S11

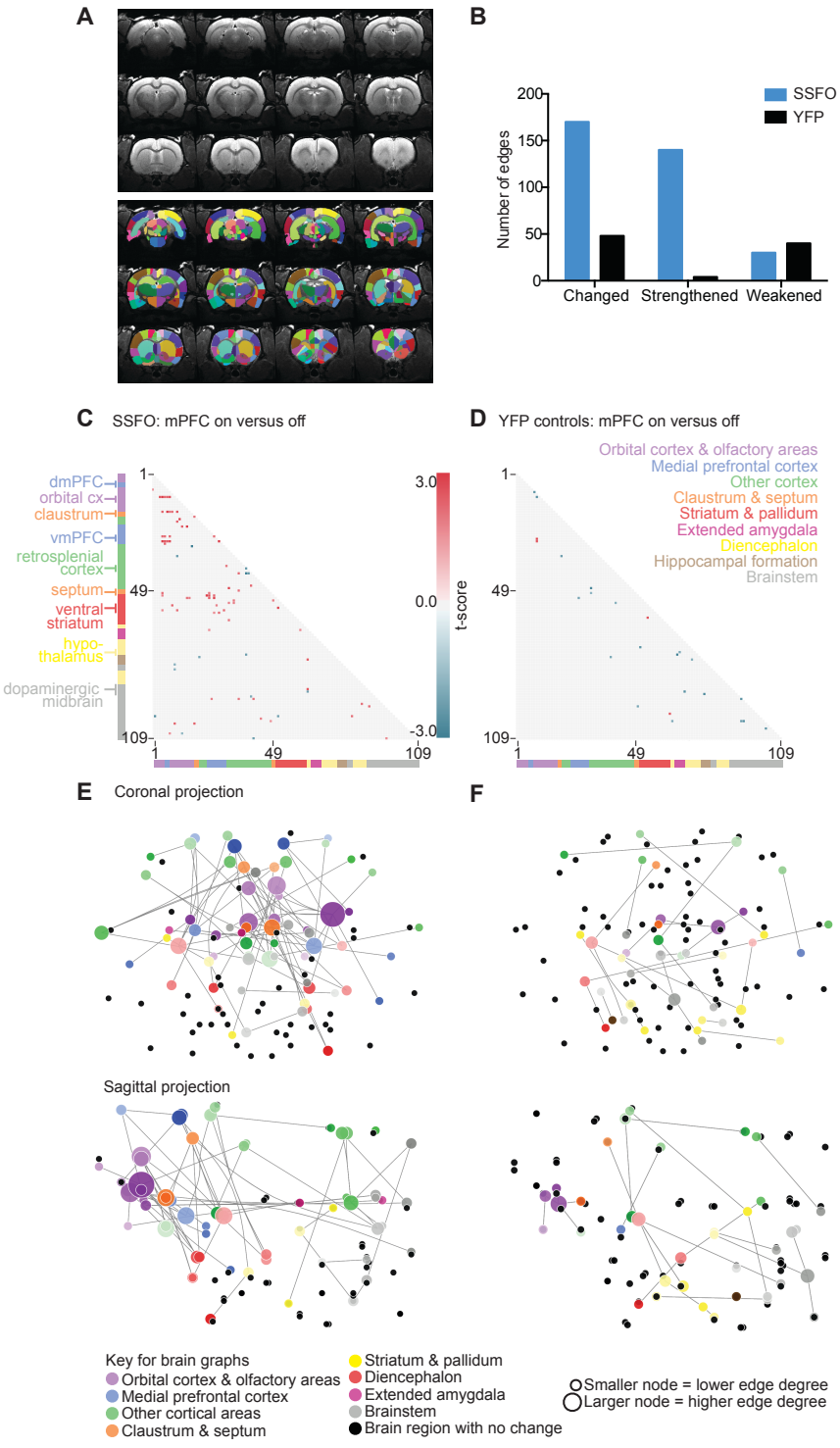
A
B
200
150
100
50
0
Number of edges
SSFO
YFP
Changed
Strengthened
Weakened
C
SSFO: mPFC on versus off
dmPFC
orbital cx
claustrum
vmPFC
retrosplenial cortex
septum
ventral striatum
hypo-thalamus
dopaminergic midbrain
1
49
109
3.0
0.0
-3.0
t-score
D
YFP controls: mPFC on versus off
Orbital cortex & olfactory areas
Medial prefrontal cortex
Other cortex
Claustrum & septum
Striatum & pallidum
Extended amygdala
Diencephalon
Hippocampal formation
Brainstem
E
Coronal projection
Sagittal projection
F
Key for brain graphs
Orbital cortex & olfactory areas
Medial prefrontal cortex
Other cortical areas
Claustrum & septum
Striatum & pallidum
Diencephalon
Extended amygdala
Brainstem
Brain region with no change
Smaller node = lower edge degree
Larger node = higher edge degree

Fig. S11

Brain-wide partial correlation analysis

A, T2-weighted anatomical template brain and manually drawn ROI atlas encompassing 109 different brain regions (guided by Paxinos and Watson Stereotactic Rat Brain Atlas) used for brain-wide partial correlation analysis. **B** Summary of number and direction of edge changes in response to mPFC activation in SSFO-expressing subjects and YFP controls. **C-F** Graphical brain-wide analysis of BOLD activity partial correlation changes between light on versus light off for SSFO-expressing subjects (4 rats, 14 runs) and YFP-control subjects (4 rats, 15 runs). Sparse partial correlation matrices were estimated using graphical lasso for each dataset (run). To perform a statistical comparison between conditions, across all subjects, we adopted the following screening threshold to control our false discovery rate: at least one value in a pairwise relationship must be non-zero in the majority (> 60%) of datasets in either condition. For the pairwise relationships that survived screening, we compared whether they were different under "opsin on" versus "opsin off" conditions by doing an element-wise permutation t-test with 1000 permutations. Graphs were thresholded for display at an uncorrected p-value < 0.05. **C**,**D**, Results of permutation testing for sparse partial correlation graphs for SSFO on versus SSFO off across all SSFO-expressing and YFP-expressing subjects. Brain regions (individual ROIs) are labeled by number, with the index key provided in Supplementary Figure 12. Colored bars indicate broad anatomical brain regions, with selected individual regions highlighted on the left-hand side. **E**,**F** Results from **C**,**D** displayed in "brain" format, using the coordinates of the center of mass of each brain region to draw "nodes" indicating individual brain regions and "edges" indicating the connections between brain regions that have changed. Color of node indicates broad anatomical brain region (with different shades denoting sub-regions), size of node indicates the number of connections (edge degrees) that changed in response to optogenetic stimulation. A black node is a brain region with no change in connections between conditions. The data displayed in this figure is available as an online analysis resource at: http://clarityresourcecenter.org/ofMRI.html. In this online resource, the data has been provided in three analysis formats: 1) as the pre-processed functional MRI scans (NIfTI), 2) the extracted BOLD timeseries for 109 regions of interest spanning the brain for each scan (Matlab), 3) the correlation and partial correlation matrices for each scan, as well as the aggregate results of the group analysis (Matlab).

Figure S12

#	ROI Name (short)	ROI Name (long)	Change in number of edges					
			SSFO			YFP		
			Total	↑	↓	Total	↑	↓
1	AO_R	Right anterior olfactory area	1	1	0	0	0	0
2	AO_L	Left anterior olfactory area	1	0	1	0	0	0
3	OB_L	Left olfactory bulb	0	0	0	0	0	0
4	OB_R	Right olfactory bulb	1	1	0	0	0	0
5	PL_R	Right prelimbic cortex	6	7	0	0	0	0
6	PL_L	Left prelimbic cortex	4	4	0	0	0	0
7	MO_R	Right medial orbital cortex	3	3	0	0	0	0
8	MO_L	Left medial orbital cortex	5	6	0	1	0	1
9	VO_R	Right ventral orbital cortex	1	2	0	3	2	2
10	VO_L	Left ventral orbital cortex	2	1	2	0	0	0
11	LO_R	Right lateral orbital cortex	8	8	1	0	0	1
12	LO_L	Left lateral orbital cortex	1	1	0	0	0	0
13	DLO_R	Right dorsolateral orbital cortex	1	1	1	0	0	0
14	DLO_L	Left dorsolateral orbital cortex	0	0	0	0	0	0
15	FrA_R	Right frontal association cortex	2	2	0	0	0	0
16	FrA_L	Left frontal association cortex	1	1	0	0	0	0
17	Cl_R	Right claustrum	4	5	1	0	0	0
18	Cl_L	Left claustrum	3	2	0	0	0	0
19	insularCx_R	Right insular cortex	4	1	0	1	0	1
20	insularCx_L	Left insular cortex	1	1	1	0	0	0
21	PirCx_R	Right piriform cortex	0	1	0	0	0	0
22	PirCx_L	Left piriform cortex	0	0	0	0	0	0
23	CingCx1_R	Right cingulate cortex area 1	3	3	0	0	0	0
24	CingCx1_L	Left cingulate cortex area 1	4	4	0	0	0	0
25	CingCx2_R	Right cingulate cortex area 2	2	1	0	0	0	0
26	CingCx2_L	Left cingulate cortex area 2	3	4	0	1	0	1
27	IL_R	Right infralimbic cortex	3	5	0	0	0	0
28	IL_L	Left infralimbic cortex	2	2	0	1	1	0
29	DP_R	Right dorsal peduncular cortex	5	5	0	1	1	0
30	DP_L	Left dorsal peduncular cortex	3	2	0	0	0	0
31	M1Cx_R	Right primary motor cortex	2	1	1	1	0	2
32	M1Cx_L	Left primary motor cortex	3	3	0	0	0	0
33	M2Cx_R	Right secondary motor cortex	0	0	0	0	0	0
34	M2Cx_L	Left secondary motor cortex	1	2	0	0	0	0
35	S1Cx_R	Right orimary sensory cortex	2	0	1	1	0	1
36	S1Cx_L	Left primary sensory cortex	1	3	0	0	0	0
37	S2Cx_R	Right secondary sensory cortex	0	0	0	0	0	0
38	S2Cx_L	Left secondary sensory cortex	0	0	0	0	0	0
39	RetrosplenCx_R	Right retrosplenial cortex	4	1	3	1	0	1
40	RetrosplenCx_L	Left retrosplenial cortex	2	0	2	0	0	0
41	AuditoryCx_R	Right auditory cortex	1	1	1	0	0	1
42	AuditoryCx_L	Left auditory cortex	4	2	3	0	0	0
43	EntorhinalCx_R	Right entorhinal cortex	0	0	0	0	0	0
44	EntorhinalCx_L	Left entorhinal cortex	0	0	0	0	0	0
45	VisualCx_R	Right visual cortex	1	1	0	0	0	0
46	VisualCx_L	Left visual cortex	0	0	0	0	0	0
47	ParietalCx_R	Right parietal cortex	1	1	0	0	0	0
48	ParietalCx_L	Left parietal cortex	1	1	0	1	0	1
49	septalRegion_R	Right septal area	0	2	0	0	0	0
50	septalRegion_L	Left septal area	3	3	0	1	0	2
51	CauPut_R	Right caudate/putamen	4	4	0	0	0	1
52	CauPut_L	Left caudate/putamen	6	5	1	2	0	1
53	GloPall_R	Right globus pallidus	1	2	0	0	0	0
54	GloPall_L	Left globus pallidus	2	2	0	1	1	1
55	NucAccSh_R	Right nucleus accumbens shell	1	2	0	0	0	0
56	NucAccSh_L	Left nucleus accumbens shell	1	1	0	0	0	0
57	NucAccCo_R	Right nucleus accumbens core	3	3	0	0	0	0
58	NucAccCo_L	Left nucleus accumbens core	3	2	0	0	0	0
59	VentPall_R	Right ventral pallidum	1	0	0	0	0	0
60	VentPall_L	Left ventral pallidum	0	0	0	1	1	0
61	medialfb_R	Right medial forebrain bundle	1	2	0	0	0	0
62	medialfb_L	Left medial forebrain bundle	0	0	0	0	0	0
63	Thalamus_R	Right thalamus	0	0	0	1	1	0
64	Thalamus_L	Left thalamus	1	2	1	0	0	1
65	BNST_R	Right bed nucleus of the stria terminalis	1	2	0	0	0	0
66	BNST_L	Left bed nucleus of the stria terminalis	0	0	0	2	0	1
67	Amygdala_R	Right amygdala	0	0	0	0	0	1
68	Amygdala_L	Left amydala	0	0	0	0	0	0
69	preopticArea_R	Right preoptic area	0	0	0	0	0	1
70	preopticArea_L	Left preoptic area	0	0	0	0	0	0
71	diagonalBand	Diagonal band	0	0	0	0	0	0
72	subInominata_R	Right substantia innominata	0	0	0	0	0	2
73	subInominata_L	Left substantia innominata	0	0	0	0	0	0
74	Hypothalamus_R	Right hypothalamus	0	0	0	0	0	1
75	Hypothalamus_L	Left hypothalamus	1	0	1	1	0	1
76	Hipp_R	Right hippocampus	0	0	1	1	0	1
77	Hipp_L	Left hippocampus	0	1	0	1	0	2

#	ROI Name (short)	ROI Name (long)	Change in number of edges					
			SSFO			YFP		
			Total	↑	↓	Total	↑	↓
78	Subiculum_R	Right subiculum	1	0	0	0	0	0
79	Subiculum_L	Left subiculum	1	0	1	0	0	0
80	Habenula_R	Right habenula	0	0	0	0	0	0
81	Habenula_L	Left habenula	1	0	1	0	0	0
82	mammillary_R	Right mammillary body	0	1	0	0	0	0
83	mammillary_L	Left mammillary body	0	0	0	0	0	0
84	STh_R	Right subthalamic nucleus	0	0	0	0	0	0
85	STh_L	Left subthalamic nucleus	0	0	0	1	0	0
86	ZI_R	Right zona incerta	1	1	0	0	0	0
87	ZI_L	Left zona incerta	0	0	0	1	0	0
88	VTA_R	Right ventral tegmental area	0	0	0	0	0	0
89	VTA_L	Left ventral tegmental area	1	2	0	0	0	0
90	SN_R	Right substantia nigra	2	0	1	0	0	1
91	SN_L	Left substantia nigra	0	0	0	1	0	1
92	PAG_R	Right periaqueductal gray	0	0	1	1	0	2
93	PAG_L	Left periaqueductal gray	3	3	0	3	0	2
94	MLF_R	Right medial longitudinal fasciculus	0	0	0	0	0	0
95	MLF_L	Left medial longitudinal fasciculus	1	1	0	1	0	0
96	RedNuc_R	Right red nucleus	2	2	0	1	0	1
97	RedNuc_L	Left red nucleus	1	0	0	0	0	0
98	pretectum_R	Right pretectal nuclei	0	0	0	0	0	0
99	pretectum_L	Left pretectal nuclei	0	0	0	1	1	0
100	SupColl_R	Right superior colliculus	1	1	2	0	0	0
101	SupColl_L	Left superior colliculus	1	1	0	0	0	0
102	Raphe	Raphe nucleus (midline)	0	1	0	2	0	4
103	InfColl_R	Right inferior colliculus	2	2	0	0	0	0
104	InfColl_L	Left inferior colliculus	0	0	0	0	0	0
105	pons_R	Right pontine nuclei	0	0	0	1	0	1
106	pons_L	Left pontine nuclei	0	0	0	0	0	0
107	CnF_R	Right cuneiform nucleus	0	1	1	0	0	0
108	CnF_L	Left cuneiform nucleus	0	0	0	0	0	0
109	pineal	Pineal gland	2	1	1	0	0	0

Fig. S12

Change in edge degree for each individual brain regions

The change in edge degree (the change in the number of significant connections with other brain regions) following light stimulation in mPFC, across all SSFO-expressing subjects (n = 4 rats, 14 runs) and all YFP-control subjects (n = 4 rats, 15 runs) for all brain regions. The figure provides a complete list of edge degree (or connection) changes for all 109 regions of interest (ROIs). These are listed in order of the ROI index number, alongside their short-form and long-form labels. The total number of changes is shown (in black), as well the breakdown of this total in terms of the direction of change i.e. the number of connections gained (shown in red, upward arrow as column heading) and number of connections lost (shown in blue, downward arrow as column heading).

Figure S13

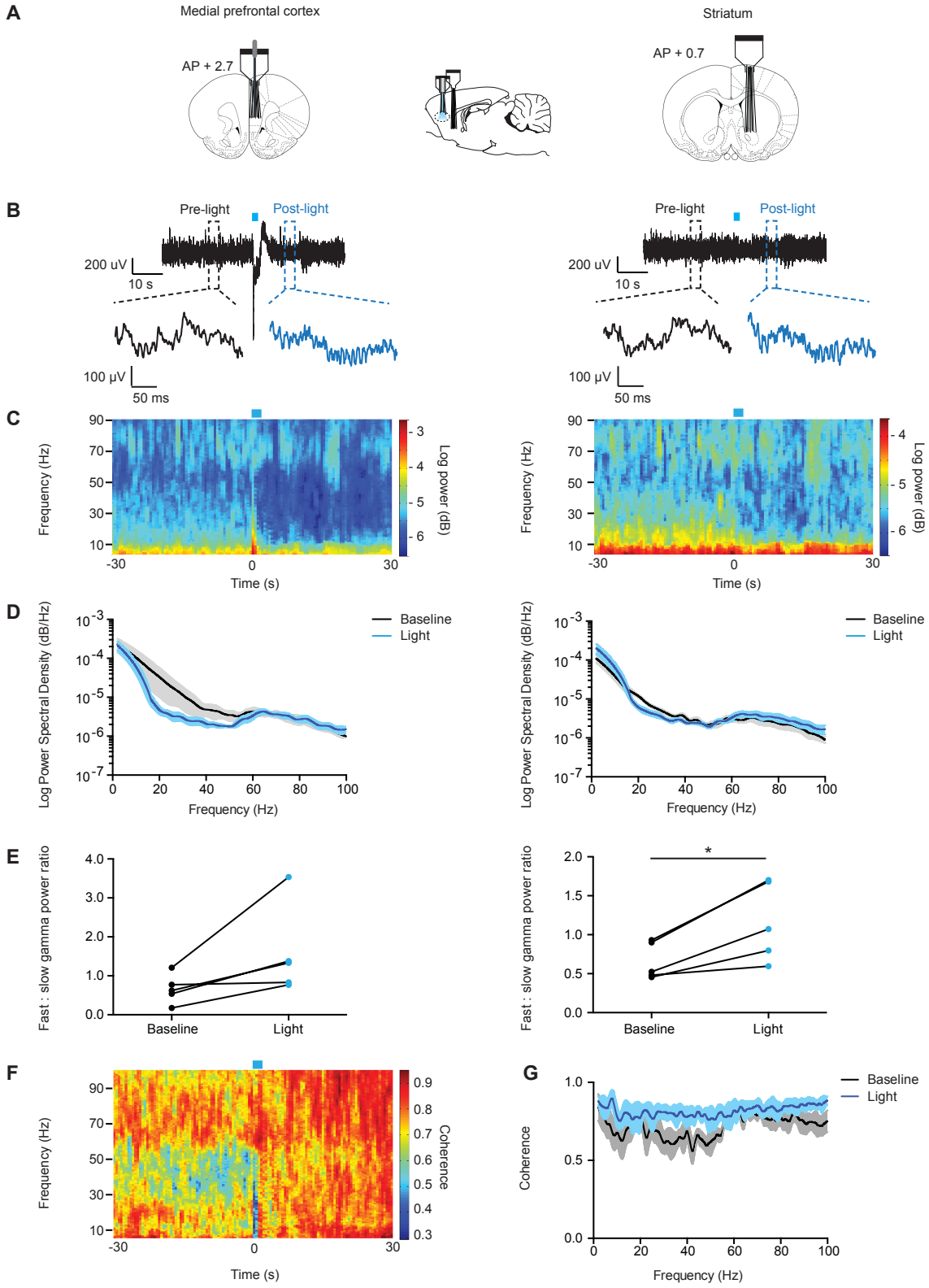
A
Medial prefrontal cortex
AP + 2.7
Striatum
AP + 0.7
B
Pre-light
Post-light
200 uV
10 s
100 µV
50 ms
C
Frequency (Hz)
Time (s)
Log power (dB)
D
Log Power Spectral Density (dB/Hz)
Frequency (Hz)
Baseline
Light
E
Fast : slow gamma power ratio
Baseline
Light
*
F
Frequency (Hz)
Time (s)
Coherence
G
Coherence
Frequency (Hz)
Baseline
Light

Fig. S13

High-frequency gamma rhythms linking distant brain-wide regions elicited by focal excitability shift in mPFC

A, Atlas images showing location of in vivo recording electrodes in medial prefrontal cortex and striatum. **B**, Example of local field potential recordings in medial prefrontal cortex (left panel) and striatum (right panel). A 2 s pulse of blue light was delivered halfway through the trace (indicated by the blue bar). Lower panels show zoom-ins of 250 ms regions of the traces, as indicated by the dashed boxes. **C**, Example spectrograms from a single subject showing changes in spectral power across the frequency range of 5 to 90 Hz over a 60 s recording for medial prefrontal cortex (left panel) and striatum (right panel). A pulse of blue light was delivered at the 0 s time point (indicated by the blue bar). **D**, Power spectral density plots (logarithmic scale) for the local field potential in medial prefrontal cortex (left panel) and striatum (right panel) at baseline (preceding the light pulse, first 5 s excluded, in black) and during SSFO activation (following the light pulse, first 5 s excluded, in blue). Mean (solid lines) and SEM (shaded regions) are shown (n = 5 subjects). **E**, Change in the ratio of fast (70-80 Hz) to slow (30-40 Hz) gamma power in medial prefrontal cortex (left panel) and striatum (right panel) from the baseline epoch (preceding light pulse, in black) to the light-activated epoch (in blue) for each subject (n = 5). This change was significant for the striatum (paired t-test, $t = 3.995$ $df = 4$, $p = 0.0162$) and showed a trend in the same direction for medial prefrontal cortex (paired t-test, $t = 2.390$ $df = 4$, $p = 0.0751$). **F**, Coherence between medial prefrontal cortex and striatum over time across a frequency range of 5 to 100 Hz. Mean coherence for 5 subjects is shown. A blue light pulse was delivered at the 0 s time point (indicated by the blue bar). **G**, Coherence between medial prefrontal cortex and striatum as a function of frequency for the baseline epoch (preceding light pulse, first 5 s excluded, in black) and the light-activated epoch (first 5 s excluded, in blue). Mean (solid line) and SEM (shaded region) are shown (n = 5 subjects).

Figure S14

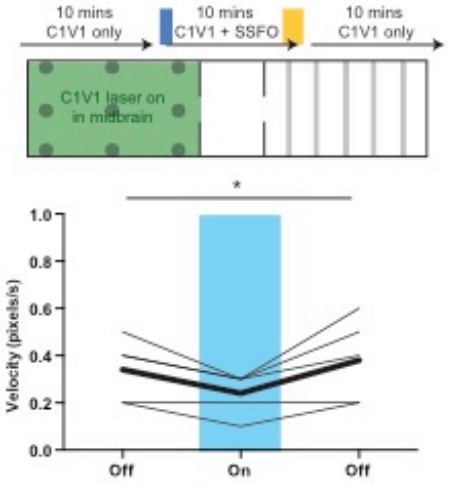
10 mins
C1V1 only
10 mins
C1V1 + SSFO
10 mins
C1V1 only
C1V1 laser on
in midbrain
*
1.0
0.8
0.6
0.4
0.2
0.0
Velocity (pixels/s)
Off
On
Off

Fig. S14

Velocity of locomotion during real-time place preference test during dual stimulation (mPFC SSFO + midbrain C1V1$_{TT}$ stimulation)

Velocity decreased during the dual stimulation condition (mPFC stimulation + midbrain dopamine neuron stimulation) compared to midbrain dopamine neuron stimulation alone (contingent on chamber entry). A one-way repeated measures ANOVA was significant ($p = 0.015$, $F(2,8) = 7.429$) with significant differences in post-hoc testing for baseline versus opsin on and washout versus opsin on comparisons using Newman-Keuls multiple comparison test. Thin lines indicate individual subjects, thick line indicates mean.

Figure S15

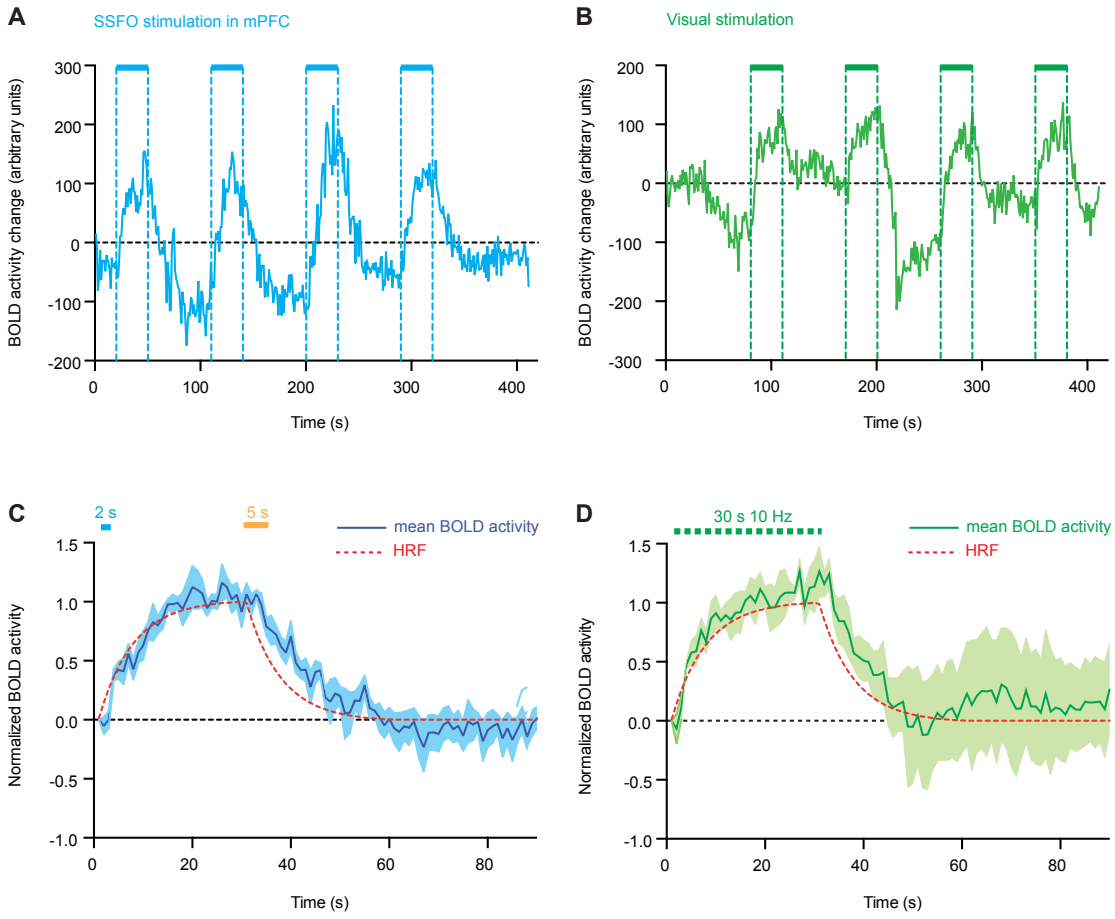
A
SSFO stimulation in mPFC
BOLD activity change (arbitrary units)
Time (s)
B
Visual stimulation
BOLD activity change (arbitrary units)
Time (s)
C
2 s
5 s
mean BOLD activity
HRF
Normalized BOLD activity
Time (s)
D
30 s 10 Hz
mean BOLD activity
HRF
Normalized BOLD activity
Time (s)

Fig. S15

mPFC and visual BOLD activity time-courses and estimated hemodynamic response function

A, Example of BOLD activity in the medial prefrontal cortex over a 420 s scan during which SSFO is stimulated using a block trial design (30 s stimulation epochs, 60 s recovery). Stimulation epochs indicated by blue horizontal bars and dashed blue vertical lines. **B**, Example of BOLD activity in the superior colliculus over the same 420 s scan during which visual stimulation is delivered (green light flashing in front of eye) using a block trial design (30 s stimulation epochs, 60 s recovery). Stimulation epochs indicated by green horizontal bars and dashed green vertical lines. **C**, Stimulation-averaged time-course for four 30 s SSFO stimulation epochs (dark blue solid line indicates mean BOLD activity in response to SSFO stimulation, light blue shaded region indicates SEM). Dashed red line indicates a custom hemodynamic response function, with exponential rise and decay (time constant = 7 s). **D**, Stimulation-averaged time-course for four 30 s visual stimulation epochs (dark green solid line indicates mean BOLD activity in response to visual stimulation, light green shaded region indicates SEM). Dashed red line represents a custom hemodynamic response function, with exponential rise and decay (time constant = 7 s).

Figure S16

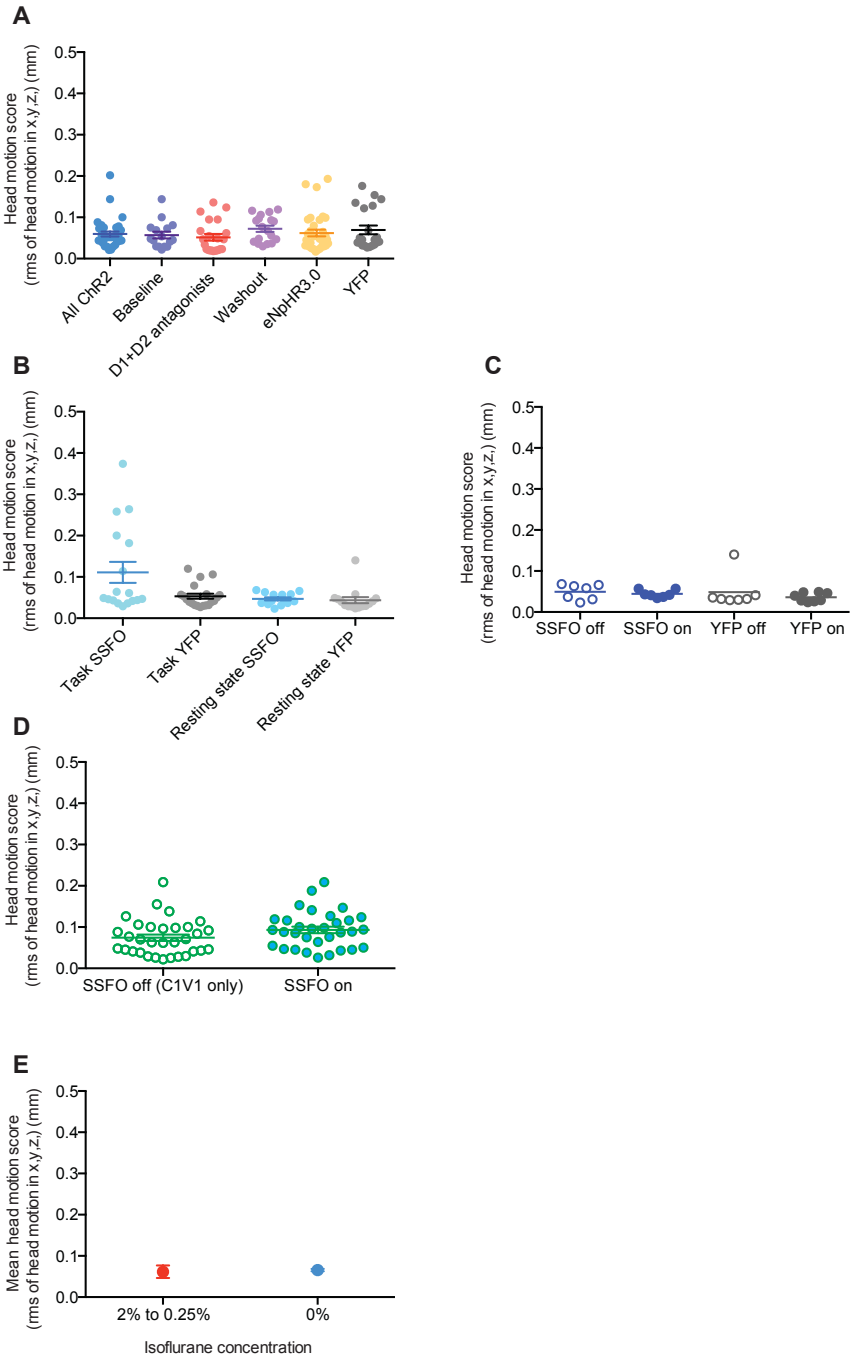
A
Head motion score
(rms of head motion in x,y,z,) (mm)
0.5
0.4
0.3
0.2
0.1
0.0
All ChR2
Baseline
D1+D2 antagonists
Washout
eNpHR3.0
YFP
B
Head motion score
(rms of head motion in x,y,z,) (mm)
Task SSFO
Task YFP
Resting state SSFO
Resting state YFP
C
Head motion score
(rms of head motion in x,y,z,) (mm)
SSFO off
SSFO on
YFP off
YFP on
D
Head motion score
(rms of head motion in x,y,z,) (mm)
SSFO off (C1V1 only)
SSFO on
E
Mean head motion score
(rms of head motion in x,y,z,) (mm)
2% to 0.25%
0%
Isoflurane concentration

Fig. S16

Head motion during awake scanning

Head motion data for all runs from all subjects used in analyses. Head motion is quantified as the root mean square (RMS) of head translation in 3 dimensions (x, y, z). **A**, Midbrain dopaminergic stimulation experiments (number of scans per condition: All ChR2 = 34, baseline = 16, drugs = 22, washout = 18, YFP = 21, eNpHR = 33). **B**, Medial prefrontal cortex experiments (task (number of scans: SSFO = 18, YFP = 20) and resting state (number of scans: SSFO = 14, YFP = 15)). **C**, Resting state experiments subdivided into mPFC stimulation ON (number of scans: SSFO = 7, YFP = 8) and OFF conditions (number of scans: SSFO = 7, YFP = 7). **D**, Dual stimulation experiments (number of scans: SSFO OFF = 32, SSFO ON = 32). **E**, Mean (+/- SEM) head motion score for anesthetized scans (number of scans = 30) and for all included awake scans (number of scans = 255).

Supplementary Tables

Table S1A

Estimated location of peak Z-score	Coordinates of peak Z-score			Max Z-score	Mean Z-score	Number of voxels	Neuroanatomical extent
	RL	DV	AP				
R hippocampus	2.5	-3.6	-3.0	4.0955	3.0312	55	R hippocampus R caudate putamen R septum R thalamus R habenula
R entorhinal cortex	5.7	-5.3	-5.0	3.7566	2.8798	13	R entorhinal cortex R caudate putamen R insular cortex R sensory cortex (S2)
L globus pallidus	-1.9	-7.5	-2.0	3.5357	2.8703	9	L globus pallidus L ventral pallidum L preoptic area L BNST L nucleus accumbens core L hypothalamus
R cingulate cortex	1.0	-2.2	3.0	3.4619	2.8334	6	R cingulate cortex R prelimbic cortex
R caudate putamen	3.6	-6.8	-1.0	3.756	2.9612	5	R caudate putamen R globus pallidus R ventral pallidum

Table S1B

Estimated location of peak Z-score	Coordinates of peak Z-score			Max Z-score	Mean Z-score	Number of voxels	Neuroanatomical extent
	RL	DV	AP				
R inferior colliculus	1.6	-3.4	-10	3.9319	2.9995	7	R inferior colliculus R retrosplenial cortex

Table S1

Midbrain dopaminergic neuron stimulation with ChR2: Anesthetized versus awake scans

Summary of regions of significant evoked BOLD contrast between ChR2-expressing rats when awake versus anesthetized in response to **A**, ChR2 stimulation of dopamine neurons (map shown in Fig. S1F) **B**, visual stimulation (map not shown). The location and coordinates of the peak Z-score of each cluster, the mean Z-score and the spatial extent of each cluster (in terms of number of functional voxels and neuroanatomical regions spanned within a cluster) are listed. Coordinates are specified in terms of right-left (R-L, where positive values are right-sided), dorso-ventral (D-V) and anterior-posterior (A-P). Please note that the coordinates provided are relative to an estimated "bregma" in our anatomical MRI reference space, determined to be as close as possible to the standard stereotactic bregma (*94*). The corresponding neuroanatomical brain regions were verified by manual inspection. The same statistical threshold was applied as for the maps ($p < 0.05$ corrected ($K > 5$ functional voxels [80 transformed voxels], uncorrected $p < 0.01$).

Table S2A

Estimated location of peak Z-score	Coordinates of peak Z-score			Max Z-score	Mean Z-score	Number of voxels	Neuroanatomical extent
	RL	DV	AP				
R caudate putamen	3.2	-4.6	1.5	5.6887	3.5525	223	R caudate putamen R claustrum R insular cortex R septum R nucleus accumbens core R thalamus
R cingulate cortex	0.4	-1.4	-0.9	3.4676	2.8772	15	R&L cingulate cortex R motor cortex
R superior colliculus	1.3	-3.7	-8.8	3.2643	2.9172	8	R superior colliculus R retrosplenial cortex
L periaqueductal gray	-0.1	-4.6	-5.6	3.8284	2.9856	5	L periaqueductal gray L superior colliculus
R ant olfactory area	1.8	-7.0	434	3.0053	2.7325	5	R anterior olfactory area

Table S2B

Estimated location of peak Z-score	Coordinates of peak Z-score			Max Z-score	Mean Z-score	Number of voxels	Neuroanatomical extent
	RL	DV	AP				
L superior colliculus	0.4	-3.6	-6.9	-5.0669	-3.2472	51	R&L superior colliculus R retrosplenial cortex R pretectum
L visual cortex	-3.3	-1.9	-7.0	4.279	3.3016	28	L visual cortex L retrosplenial cortex
R thalamus	3.3	-4.8	-4.4	-3.4202	-2.8153	13	R thalamus
L thalamus	-1.9	-4.3	-4.6	-3.256	-2.9053	9	L thalamus
R inferior colliculus	0.7	-4.3	-8.8	3.2023	2.847	8	R inferior colliculus
L cingulate cortex	-0.9	-1.6	0.0	-3.3266	-2.907	5	L cingulate cortex L motor cortex
R sensory cortex (S1)	5.1	-2.1	-1.5	-3.4058	-2.8992	5	R sensory cortex (S1)

Table S2

Midbrain dopaminergic neuron stimulation: ChR2-expressing rats versus YFP control rats

Summary of regions of significant evoked BOLD contrast between ChR2-expressing rats and YFP control rats in response to **A**, ChR2 stimulation of dopamine neurons (map shown in Fig. S3A) **B**, visual stimulation (map shown in Fig. S3B). The location and coordinates of the peak Z-score of each cluster, the mean Z-score and the spatial extent of each cluster (in terms of number of functional voxels and neuroanatomical regions spanned within a cluster) are listed. Coordinates are specified in terms of right-left (R-L, where positive values are right-sided), dorso-ventral (D-V) and anterior-posterior (A-P). Please note that the coordinates provided are relative to an estimated "bregma" in our anatomical MRI reference space, determined to be as close as possible to the standard stereotactic bregma (*94*). The corresponding neuroanatomical brain regions were verified by manual inspection. The same statistical threshold was applied as for the maps ($p < 0.05$ corrected ($K > 5$ functional voxels [80 transformed voxels], uncorrected $p < 0.01$).

Table S3A

Estimated location of peak Z-score	Coordinates of peak Z-score			Max Z-score	Mean Z-score	Number of voxels	Neuroanatomical extent
	RL	DV	AP				
R nucleus acc core	1.8	-7.5	1.9	-4.6953	-3.1421	138	R nucleus acc core R nucleus acc shell R ventral orbital cortex R claustrum R septum R caudate-putamen R globus pallidus R thalamus R hippocampus R piriform cortex
R claustrum	2.7	-4.2	2.4	-2.9994	-2.7874	7	R claustrum
L sensory cortex (S1)	-2.4	-2.8	-1.3	-3.0517	-2.7975	6	L sensory cortex (S1)
L nucleus acc shell	-0.6	-7.9	1.9	-3.3	-2.864	6	L nucleus acc shell L nucleus acc core
R midbrain	3.2	-7.5	-6.0	-3.247	-2.8146	5	R midbrain

Table S3B

Estimated location of peak Z-score	Coordinates of peak Z-score			Max Z-score	Mean Z-score	Number of voxels	Neuroanatomical extent
	RL	DV	AP				
R thalamus	3.2	-5.1	-4.6	6.2445	3.8128	337	R&L thalamus R&L hippocampus R&L habenula
R sensory cortex (S1)	4.6	-2.8	1.9	4.5565	2.9568	18	R sensory cortex (S1) R motor cortex
R inferior colliculus	2.7	-5.1	-9.3	-3.6643	-2.8676	5	R inferior colliculus

Table S3.

Midbrain dopaminergic neuron stimulation with ChR2: Dopamine receptor antagonists versus baseline

Summary of regions of significant evoked BOLD contrast between ChR2-expressing rats during systemic administration of D1 and D2 receptor antagonists versus at baseline (no drugs) for **A**, ChR2 stimulation of dopamine neurons (map shown in Fig. 3D) **B**, visual stimulation (map shown in Fig 3D). The location and coordinates of the peak Z-score of each cluster, the mean Z-score and the spatial extent of each cluster (in terms of number of functional voxels and neuroanatomical regions spanned within a cluster) are listed. Coordinates are specified in terms of right-left (R-L, where positive values are right-sided), dorso-ventral (D-V) and anterior-posterior (A-P). Please note that the coordinates provided are relative to an estimated "bregma" in our anatomical MRI reference space, determined to be as close as possible to the standard stereotactic bregma (*94*). The corresponding neuroanatomical brain regions were verified by manual inspection. The same statistical threshold was applied as for the maps ($p < 0.05$ corrected ($K > 5$ functional voxels [80 transformed voxels], uncorrected $p < 0.01$).

Table S4A

Estimated location of peak Z-score	Coordinates of peak Z-score			Max Z-score	Mean Z-score	Number of voxels	Neuroanatomical extent
	RL	DV	AP				
R caudate putamen	2.7	-6.1	1.5	-4.8988	-3.225	204	R caudate putamen R nucleus acc shell R nucleus accumbens core R habenula R thalamus R hippocampus R infralimbic cortex R globus pallidus R claustrum R insular Ctx R dorsal peduncular Ctx
L superior colliculus	-0.1	-3.7	-7.4	-4.6171	-3.0865	49	R&L sup colliculus R&L retrosplenial cortex B&L periacqueductal gray R&L subiculum
L retrosplenial cortex	-1.5	-2.3	-7.0	-4.2771	-3.0571	22	L retrosplenial cortex L superior colliculus
R cingulate cortex	1.3	-2.8	2.4	-4.0011	-3.162	20	R cingulate cortex R prelimbic cortex R motor cortex
L motor cortex	-2.9	-1.8	-2.7	-3.7702	-3.056	20	L motor cortex L sensory cortex (S1)
L hippocampus	-3.8	-4.6	-5.6	-3.5663	-2.8351	14	L hippocampus
L ventral orbital cortex	-1.5	-5.6	2.9	-3.8727	-3.0788	10	L ventral orbital cortex L medial orbital cortex L claustrum L nucleus acc shell
R thalamus	2.7	-7.0	-4.1	-3.3843	-2.8869	7	R thalamus
L cingulate cortex	-0.1	-1.8	1.0	-3.3694	-3.0464	5	L cingulate cortex L motor cortex
R motor cortex	2.7	-0.9	1.9	-3.3796	-2.9099	5	R motor cortex

Table S4B

Estimated location of peak Z-score	Coordinates of peak Z-score			Max Z-score	Mean Z-score	Number of voxels	Neuroanatomical extent
	RL	DV	AP				
L thalamus	-2.9	-4.6	-4.1	5.8769	3.5431	209	L thalamus L hippocampus R&L subiculum L pretectum L superior colliculus
R thalamus	3.2	-5.1	-4.6	4.831	3.4265	34	R thalamus R hippocampus
L pretectum	-1.0	-6.5	-6.0	-3.359	2.7889	8	L pretectum L periacqueductal gray
L thalamus	-2.4	-6.5	-4.6	-3.3198	-2.8741	7	L thalamus
R sensory cortex (S1)	4.1	-3.2	1.9	3.7515	3.1414	6	R sensory cortex (S1)

Table S4.

Midbrain dopaminergic neuron stimulation with ChR2: Dopamine receptor antagonists versus washout

Summary of regions of significant evoked BOLD contrast between ChR2-expressing rats during systemic administration of D1 and D2 receptor antagonists versus after "washout" (systemic vehicle control injection 24-48 hours post-drug administration) for **A**, ChR2 stimulation of dopamine neurons (map shown in Fig. 3D) **B**, visual stimulation (map shown in Fig 3D). The location and coordinates of the peak Z-score of each cluster, the mean Z-score and the spatial extent of each cluster (in terms of number of functional voxels and neuroanatomical regions spanned within a cluster) are listed. Coordinates are specified in terms of right-left (R-L, where positive values are right-sided), dorso-ventral (D-V) and anterior-posterior (A-P). Please note that the coordinates provided are relative to an estimated "bregma" in our anatomical MRI reference space, determined to be as close as possible to the standard stereotactic bregma (*94*). The corresponding neuroanatomical brain regions were verified by manual inspection. The same statistical threshold was applied as for the maps ($p < 0.05$ corrected ($K > 5$ functional voxels [80 transformed voxels], uncorrected $p < 0.01$).

Table S5A

Estimated location of peak Z-score	Coordinates of peak Z-score			Max Z-score	Mean Z-score	Number of voxels	Neuroanatomical extent
	RL	DV	AP				
R infralimbic cortex	0.8	-5.0	3.0	3.9038	3.085	43	R&L infralimbic cortex R&L prelimbic cortex R ventral orbital cortex

Table S5B

Estimated location of peak Z-score	Coordinates of peak Z-score			Max Z-score	Mean Z-score	Number of voxels	Neuroanatomical extent
	RL	DV	AP				
R retrosplenial cortex	1.4	-3.3	-7.0	3.4268	2.8669	8	R retrosplenial cortex R visual cortex
R hippocampus	5.5	-4.5	-6.0	4.018	3.2347	7	R hippocampus R subiculum

Table S5.

Event-related mPFC stimulation: SSFO-expressing rats versus YFP control rats

Summary of regions of significant evoked BOLD contrast between SSFO-expressing rats and YFP control rats in response to **A**, SSFO stimulation of glutamatergic neurons in the medial prefrontal cortex (mPFC) (map shown in Fig. S9A) **B**, visual stimulation (map shown in Fig. S9B). The location and coordinates of the peak Z-score of each cluster, the mean Z-score and the spatial extent of each cluster (in terms of number of functional voxels and neuroanatomical regions spanned within a cluster) are listed. Coordinates are specified in terms of right-left (R-L, where positive values are right-sided), dorso-ventral (D-V) and anterior-posterior (A-P). Please note that the coordinates provided are relative to an estimated "bregma" in our anatomical MRI reference space, determined to be as close as possible to the standard stereotactic bregma (*94*). The corresponding neuroanatomical brain regions were verified by manual inspection. The same statistical threshold was applied as for the maps ($p < 0.05$ corrected ($K > 5$ functional voxels [80 transformed voxels], uncorrected $p < 0.01$).

Table S6A

Estimated location of peak Z-score	Coordinates of peak Z-score			Max Z-score	Mean Z-score	Number of voxels	Neuroanatomical extent
	RL	DV	AP				
R caudate putamen	1.6	-4.1	1.0	-4.0276	-3.0876	19	R caudate putamen R claustrum

Table S6B

Estimated location of peak Z-score	Coordinates of peak Z-score			Max Z-score	Mean Z-score	Number of voxels	Neuroanatomical extent
	RL	DV	AP				
R corpus callosum	1.7	-3.3	-1.0	-4.652	-3.2879	8	R corpus callosum R caudate putamen
L thalamus	-2.1	-5.4	-3.0	-3.708	-2.929	7	L thalamus

Table S6.

Dual stimulation experiment with C1V1$_{TT}$ in midbrain dopamine neurons: SSFO activation of mPFC versus no activation

Summary of regions of significant evoked BOLD contrast between SSFO activation of mPFC versus no mPFC activation during **A**, C1V1$_{TT}$-mediated stimulation of midbrain dopamine neurons (map shown in Fig. 5F) **B**, visual stimulation (map shown in Fig. 5F). The location and coordinates of the peak Z-score of each cluster, the mean Z-score and the spatial extent of each cluster (in terms of number of functional voxels and neuroanatomical regions spanned within a cluster) are listed. Coordinates are specified in terms of right-left (R-L, where positive values are right-sided), dorso-ventral (D-V) and anterior-posterior (A-P). Please note that the coordinates provided are relative to an estimated "bregma" in our anatomical MRI reference space, determined to be as close as possible to the standard stereotactic bregma (*94*). The corresponding neuroanatomical brain regions were verified by manual inspection. The same statistical threshold was applied as for the maps ($p < 0.05$ corrected ($K > 5$ functional voxels [80 transformed voxels], uncorrected $p < 0.01$).

Table S7

Estimated location of peak Z-score	Coordinates of peak Z-score			Max Z-score	Mean Z-score	Number of voxels	Neuroanatomical extent
	RL	**DV**	**AP**				
R lateral orbital cortex	2.8	-4.9	3.0	4.7329	3.0766	643	R&L lateral orbital cortex R&L medial orbital cortex R&L ventral orbital cortex R&L prelimbic cortex R&L infralimbic cortex R&L cingulate cortex R&L motor cortex L frontal association ctx R&L ventral pallidum R&L nucleus acc core R&L nucleus acc shell R&L caudate putamen R&L globus pallidus R&L septum R&L dorsal peduncular cx R&L claustrum R medial forebrain bundle R preoptic area R sensory cortex (S1) R&L insular cortex R&L hippocampus R& piriform cortex R amygdala R BNST R&L pons R&L thalamus R subthalamic nucleus
R retrosplenial cortex	1.3	-2.3	-8.0	4.2223	2.9459	55	R&L retrosplenial cortex R&L inferior colliculus R entorhinal crotex R subiculum
L inferior colliculus	-2.0	-5.6	-8.0	3.3296	2.8191	10	L inferior colliculus L subiculum
L subiculum	-2.5	-3.8	-7.0	3.302	2.7934	6	L subiculum L retrosplenial cortex

Table S7.

Resting state experiments with mPFC stimulation with SSFO: SSFO-expressing rats versus YFP control rats

Summary of regions exhibiting significant changes in resting state functional connectivity (BOLD activity correlations) seeded from the mPFC after opsin activation in SSFO-expressing rats compared to YFP control rats (map shown in Fig. S9C). The location and coordinates of the peak Z-score of each cluster, the mean Z-score and the spatial extent of each cluster (in terms of number of functional voxels and neuroanatomical regions spanned within a cluster) are listed. Coordinates are specified in terms of right-left (R-L, where positive values are right-sided), dorso-ventral (D-V) and anterior-posterior (A-P). Please note that the coordinates provided are relative to an estimated "bregma" in our anatomical MRI reference space, determined to be as close as possible to the standard stereotactic bregma (*94*). The corresponding neuroanatomical brain regions were verified by manual inspection. The same statistical threshold was applied as for the maps ($p < 0.05$ corrected ($K > 5$ functional voxels [80 transformed voxels], uncorrected $p < 0.01$).

Supplementary Data S1

Online data resource information and instructions

The data is available as a zipped file at: http://clarityresourcecenter.org/ofMRI.html

The following information and instructions are also available online in the README.txt file)

The online mineable dataset is organized into 3 sub-folders: 1) FunctionalData_Preprocessed, 2) TimeseriesData_MotionCorrected, 3) CorrelationAndPartialCorrelationAnalysis

1) FunctionalData_Preprocessed: functional MRI data files in NIfTI (.nii.gz) format.

These MRI files have been preprocessed as described above in the methods (also provided below for ease of reference) and warped to a reference anatomical scan. The anatomical reference scan (skull stripped and non-skull stripped versions) and a mask have been provided with the functional dataset. To extract timeseries from different brain regions we have also provided an "ROI atlas", which contains 109 different ROIs. An example script from AFNI to extract these timeseries is provided. A key to the label of the anatomical brain region is provided: these are listed from numbers 1 to 109, corresponding to each of the ROIs. (Please note: in the ROI atlas - the range of intensity values for different ROIs goes from 1 to 111 - this is because two intensity values (numbers 3 and 4) have been removed (determined to be "non-brain") - therefore the sequence of values skips from 1,2 directly to 5,6. Thus intensity values 5 and 6 correspond to ROI indices 3 and 4, and so on throughout the rest of the ROIs. There are no other gaps in the sequence. Therefore, for ROI numbering, use the row index of the extracted timeseries). Each rat and each scan (also known as a run) has been labeled for unique identification. There are 4 different SSFO-expressing rats (RatA, RatB, RatC, RatD), and each rat has had multiple scans: one or more with blue light activation (SSFO_ON) and one or more with no light activation (SSFO_OFF). Scans labeled SSFO_ON or SSFO_OFF therefore represent different scans (or runs) within the same scanning session, and correspond to the blue light activation status of that scan e.g. SSFO_ON_RatA_run1. There are 4 different YFP control rats (RatW, RatZ, RatY, RatZ), and each rat has multiple scans: one or more with sham blue light activation (YFP_ON) and one or more with no sham light activation (YFP_OFF). Scans labeled YFP_ON or YFP_OFF therefore represent different scans (or runs) within the same scanning session, and correspond to the blue light sham activation status of that scan e.g. YFP_ON_RatZ_run1.

2) TimeseriesData_MotionCorrected: extracted ROI timeseries data

We have extracted the timeseries for each ROI, for each individual rat and scan (or run) (MRI scans underwent the preprocessing described below). These timeseries are provided as Matlab Matlab workspaces, which contain variables representing the individual runs, and each variable containing all the ROI timeseries for each run. The variables are row/column matrices, where the rows represent the timeseries for individual ROIs (the row index of these variables corresponds to the ROI number given in the ROI label file) and the columns indicate time points (or samples). The sampling frequency is 0.5 s. There are 600 time points, thus spanning the 300 s scan duration. Zero values in the timeseries are ones that have been censored out by the motion censor, at a threshold of 0.075 mm. The first two time points of each scan (1 s) have also been censored. We have provided the index key with the anatomical brain region label for each ROI ("ROILabels", with long form and short form labels), and the center of mass of each ROI, given in the template brain coordinates.

3) CorrelationAndPartialCorrelationAnalysis: correlation and partial correlation data analysis using graphical lasso

Here we provide the results of our correlation and partial correlation data analysis, using graph estimation with graphical lasso (please see Methods section for further details). This includes the individual correlation matrices and partial correlation matrices for each individual scan (run) as well as the group statistics across all rats following element-wise permutation testing (1000 permutations, $p < 0.05$ uncorrected). These files were exported with default settings for using Scipy.io.savemat.

Notes on fMRI pre-processing

Analysis was performed using Analysis for Functional NeuroImages (AFNI, NIMH, Bethesda MD). Scans were only included in the awake analysis if isoflurane level was 0% and an increase in respiratory rate to > 100 breaths per minute had occurred, as it took several minutes for the rats to transition from the anesthetized to the awake state. Only runs with minimal motion (maximum root mean squared displacement < 0.3 mm) were included in the functional connectivity analysis. To control for motion artifacts, we censored high-motion volumes (root

mean squared displacement > 0.075 mm), and regressed on 12 motion parameters (roll, pitch, yaw, translation in 3 dimensions, and the first derivative of each of those six parameters). Each functional scan was motion corrected, smoothed using a 0.5 mm FMWH Gaussian blur (note voxel size of 0.47 mm), normalized to the average BOLD activity over the entire scan within each voxel, and temporally bandpass filtered using a Fast Fourier Transform (FFT) bandpass filter spanning 0.005–0.1 Hz, and linear and quadratic trends were removed from the data. Data were pre-whitened to remove autocorrelation. Each subject's anatomical scan was aligned to a reference scan (manually chosen by the experimenter for high quality) using a twelve parameter affine transformation (scaling, rotation, shear), and the transformation matrix was applied to each functional scan. Aligned images were then manually inspected for consistent positioning, using the fiber insertion site, cortical contours, and other anatomical landmarks as references.

Notes on head motion

Here we provide the root mean square in mm (across x, y, z dimensions) of head motion for each resting state scan included in the online data resource.

SSFO OFF:

Scan name	Head motion (rms in mm)
SSFO_OFF_RatA_run1	0.066
SSFO_OFF_RatA_run2	0.058
SSFO_OFF_RatA_run3	0.063
SSFO_OFF_RatB_run1	0.068
SSFO_OFF_RatC_run1	0.037
SSFO_OFF_RatD_run1	0.023
SSFO_OFF_RatD_run2	0.031

SSFO ON:

Scan name	Head motion (rms in mm)
SSFO_ON_RatA_run1	0.042
SSFO_ON_RatA_run2	0.041
SSFO_ON_RatB_run1	0.057

SSFO_ON_RatC_run1	0.034
SSFO_ON_RatC_run2	0.057
SSFO_ON_RatD_run1	0.043
SSFO_ON_RatD_run2	0.037

YFP OFF:

Scan name	Head motion (rms in mm)
YFP_OFF_RatW_run1	0.032
YFP_OFF_RatW_run2	0.035
YFP_OFF_RatX_run1	0.029
YFP_OFF_RatX_run2	0.03
YFP_OFF_RatY_run1	0.140
YFP_OFF_RatZ_run1	0.041
YFP_OFF_RatZ_run2	0.032

YFP ON:

Scan name	Head motion (rms in mm)
YFP_ON_RatW_run1	0.046
YFP_ON_RatW_run2	0.029
YFP_ON_RatX_run1	0.026
YFP_ON_RatX_run2	0.049
YFP_ON_RatY_run1	0.028
YFP_ON_RatY_run2	0.024
YFP_ON_RatZ_run1	0.048
YFP_ON_RatZ_run2	0.040

References and Notes

1. A. E. Kelley, K. C. Berridge, The neuroscience of natural rewards: Relevance to addictive drugs. *J. Neurosci.* **22**, 3306–3311 (2002). Medline

2. W. Schultz, Predictive reward signal of dopamine neurons. *J. Neurophysiol.* **80**, 1–27 (1998). Medline

3. S. R. Sesack, A. A. Grace, Cortico-basal ganglia reward network: Microcircuitry. *Neuropsychopharmacology* **35**, 27–47 (2010). Medline doi:10.1038/npp.2009.93

4. M. W. Howe, P. L. Tierney, S. G. Sandberg, P. E. M. Phillips, A. M. Graybiel, Prolonged dopamine signalling in striatum signals proximity and value of distant rewards. *Nature* **500**, 575–579 (2013). Medline doi:10.1038/nature12475

5. C. D. Fiorillo, P. N. Tobler, W. Schultz, Discrete coding of reward probability and uncertainty by dopamine neurons. *Science* **299**, 1898–1902 (2003). Medline doi:10.1126/science.1077349

6. P. Gorwood, Neurobiological mechanisms of anhedonia. *Dialogues Clin. Neurosci.* **10**, 291–299 (2008). Medline

7. E. J. Nestler, W. A. Carlezon Jr., The mesolimbic dopamine reward circuit in depression. *Biol. Psychiatry* **59**, 1151–1159 (2006). Medline doi:10.1016/j.biopsych.2005.09.018

8. S. J. Russo, E. J. Nestler, The brain reward circuitry in mood disorders. *Nat. Rev. Neurosci.* **14**, 609–625 (2013). Medline doi:10.1038/nrn3381

9. K. Deisseroth, Circuit dynamics of adaptive and maladaptive behaviour. *Nature* **505**, 309–317 (2014). Medline doi:10.1038/nature12982

10. B. Moghaddam, J. Wood, Teamwork matters: Coordinated neuronal activity in brain systems relevant to psychiatric disorders. *JAMA Psychiatry* **71**, 197–199 (2014). Medline doi:10.1001/jamapsychiatry.2013.2080

11. H. S. Mayberg, A. M. Lozano, V. Voon, H. E. McNeely, D. Seminowicz, C. Hamani, J. M. Schwalb, S. H. Kennedy, Deep brain stimulation for treatment-resistant depression. *Neuron* **45**, 651–660 (2005). Medline doi:10.1016/j.neuron.2005.02.014

12. R. T. Dunn, T. A. Kimbrell, T. A. Ketter, M. A. Frye, M. W. Willis, D. A. Luckenbaugh, R. M. Post, Principal components of the Beck Depression Inventory and regional cerebral metabolism in unipolar and bipolar depression. *Biol. Psychiatry* **51**, 387–399 (2002). Medline doi:10.1016/S0006-3223(01)01244-6

13. M. T. Mitterschiffthaler, V. Kumari, G. S. Malhi, R. G. Brown, V. P. Giampietro, M. J. Brammer, J. Suckling, L. Poon, A. Simmons, C. Andrew, T. Sharma, Neural response to pleasant stimuli in anhedonia: An fMRI study. *Neuroreport* **14**, 177–182 (2003). Medline doi:10.1097/00001756-200302100-00003

14. V. Kumari, M. T. Mitterschiffthaler, J. D. Teasdale, G. S. Malhi, R. G. Brown, V. Giampietro, M. J. Brammer, L. Poon, A. Simmons, S. C. Williams, S. A. Checkley, T. Sharma, Neural abnormalities during cognitive generation of affect in treatment-resistant depression. *Biol. Psychiatry* **54**, 777–791 (2003). Medline doi:10.1016/S0006-3223(02)01785-7

15. P. A. Keedwell, C. Andrew, S. C. R. Williams, M. J. Brammer, M. L. Phillips, The neural correlates of anhedonia in major depressive disorder. *Biol. Psychiatry* **58**, 843–853 (2005). Medline doi:10.1016/j.biopsych.2005.05.019

16. P.-O. Harvey, J. Pruessner, Y. Czechowska, M. Lepage, Individual differences in trait anhedonia: A structural and functional magnetic resonance imaging study in non-clinical subjects. *Mol. Psychiatry* **12**, 767–775 (2007). Medline

17. K. J. Ressler, H. S. Mayberg, Targeting abnormal neural circuits in mood and anxiety disorders: From the laboratory to the clinic. *Nat. Neurosci.* **10**, 1116–1124 (2007). Medline doi:10.1038/nn1944

18. M. T. Berlim, A. McGirr, F. Van den Eynde, M. P. A. Fleck, P. Giacobbe, Effectiveness and acceptability of deep brain stimulation (DBS) of the subgenual cingulate cortex for treatment-resistant depression: A systematic review and exploratory meta-analysis. *J. Affect. Disord.* **159**, 31–38 (2014). Medline doi:10.1016/j.jad.2014.02.016

19. J. P. O'Doherty, Reward representations and reward-related learning in the human brain: Insights from neuroimaging. *Curr. Opin. Neurobiol.* **14**, 769–776 (2004). Medline doi:10.1016/j.conb.2004.10.016

20. B. Knutson, J. C. Cooper, Functional magnetic resonance imaging of reward prediction. *Curr. Opin. Neurol.* **18**, 411–417 (2005). Medline doi:10.1097/01.wco.0000173463.24758.f6

21. E. S. Boyden, F. Zhang, E. Bamberg, G. Nagel, K. Deisseroth, Millisecond-timescale, genetically targeted optical control of neural activity. *Nat. Neurosci.* **8**, 1263–1268 (2005). Medline doi:10.1038/nn1525

22. V. Gradinaru, K. R. Thompson, K. Deisseroth, eNpHR: A *Natronomonas* halorhodopsin enhanced for optogenetic applications. *Brain Cell Biol.* **36**, 129–139 (2008). Medline doi:10.1007/s11068-008-9027-6

23. O. Yizhar, L. E. Fenno, M. Prigge, F. Schneider, T. J. Davidson, D. J. O'Shea, V. S. Sohal, I. Goshen, J. Finkelstein, J. T. Paz, K. Stehfest, R. Fudim, C. Ramakrishnan, J. R. Huguenard, P. Hegemann, K. Deisseroth, Neocortical excitation/inhibition balance in information processing and social dysfunction. *Nature* **477**, 171–178 (2011). Medline doi:10.1038/nature10360

24. N. D. Woodward, C. J. Cascio, Resting-state functional connectivity in psychiatric disorders. *JAMA Psychiatry* **72**, 743–744 (2015). Medline doi:10.1001/jamapsychiatry.2015.0484

25. A. Berndt, O. Yizhar, L. A. Gunaydin, P. Hegemann, K. Deisseroth, Bi-stable neural state switches. *Nat. Neurosci.* **12**, 229–234 (2009). Medline doi:10.1038/nn.2247

26. I. N. Christie, J. A. Wells, P. Southern, N. Marina, S. Kasparov, A. V. Gourine, M. F. Lythgoe, fMRI response to blue light delivery in the naïve brain: Implications for combined optogenetic fMRI studies. *Neuroimage* **66**, 634–641 (2013). Medline doi:10.1016/j.neuroimage.2012.10.074

27. F. Zhang, M. Prigge, F. Beyrière, S. P. Tsunoda, J. Mattis, O. Yizhar, P. Hegemann, K. Deisseroth, Red-shifted optogenetic excitation: A tool for fast neural control derived from *Volvox carteri*. *Nat. Neurosci.* **11**, 631–633 (2008). Medline doi:10.1038/nn.2120

28. M. A. Pisauro, N. T. Dhruv, M. Carandini, A. Benucci, Fast hemodynamic responses in the visual cortex of the awake mouse. *J. Neurosci.* **33**, 18343–18351 (2013). Medline doi:10.1523/JNEUROSCI.2130-13.2013

29. H.-C. Tsai, F. Zhang, A. Adamantidis, G. D. Stuber, A. Bonci, L. de Lecea, K. Deisseroth, Phasic firing in dopaminergic neurons is sufficient for behavioral conditioning. *Science* **324**, 1080–1084 (2009). Medline doi:10.1126/science.1168878

30. I. B. Witten, E. E. Steinberg, S. Y. Lee, T. J. Davidson, K. A. Zalocusky, M. Brodsky, O. Yizhar, S. L. Cho, S. Gong, C. Ramakrishnan, G. D. Stuber, K. M. Tye, P. H. Janak, K. Deisseroth, Recombinase-driver rat lines: Tools, techniques, and optogenetic application to dopamine-mediated reinforcement. *Neuron* **72**, 721–733 (2011). Medline doi:10.1016/j.neuron.2011.10.028

31. N. K. Logothetis, J. Pauls, M. Augath, T. Trinath, A. Oeltermann, Neurophysiological investigation of the basis of the fMRI signal. *Nature* **412**, 150–157 (2001). Medline doi:10.1038/35084005

32. K. M. Tye, J. J. Mirzabekov, M. R. Warden, E. A. Ferenczi, H. C. Tsai, J. Finkelstein, S. Y. Kim, A. Adhikari, K. R. Thompson, A. S. Andalman, L. A. Gunaydin, I. B. Witten, K. Deisseroth, Dopamine neurons modulate neural encoding and expression of depression-related behaviour. *Nature* **493**, 537–541 (2013). Medline doi:10.1038/nature11740

33. G. H. Glover, S. K. Lemieux, M. Drangova, J. M. Pauly, Decomposition of inflow and blood oxygen level-dependent (BOLD) effects with dual-echo spiral gradient-recalled echo (GRE) fMRI. *Magn. Reson. Med.* **35**, 299–308 (1996). Medline doi:10.1002/mrm.1910350306

34. J. A. Bourne, SCH 23390: The first selective dopamine D_1-like receptor antagonist. *CNS Drug Rev.* **7**, 399–414 (2001). Medline doi:10.1111/j.1527-3458.2001.tb00207.x

35. S. P. S, R. R. Punde, M. Gupta, A. Dixit, S. Giri, S. Rajagopal, R. Mullangi, A highly sensitive LC-MS/MS method for the determination of *S*-raclopride in rat plasma: Application to a pharmacokinetic study in rats. *Biomed. Chromatogr.* **25**, 930–937 (2011). Medline doi:10.1002/bmc.1547

36. B. Noudoost, T. Moore, Control of visual cortical signals by prefrontal dopamine. *Nature* **474**, 372–375 (2011). Medline doi:10.1038/nature09995

37. J. T. Arsenault, K. Nelissen, B. Jarraya, W. Vanduffel, Dopaminergic reward signals selectively decrease fMRI activity in primate visual cortex. *Neuron* **77**, 1174–1186 (2013). Medline doi:10.1016/j.neuron.2013.01.008

38. D. Zaldivar, A. Rauch, K. Whittingstall, N. K. Logothetis, J. Goense, Dopamine-induced dissociation of BOLD and neural activity in macaque visual cortex. *Curr. Biol.* **24**, 2805–2811 (2014). Medline doi:10.1016/j.cub.2014.10.006

39. F. De Martino, G. Valente, N. Staeren, J. Ashburner, R. Goebel, E. Formisano, Combining multivariate voxel selection and support vector machines for mapping and classification of fMRI spatial patterns. *Neuroimage* **43**, 44–58 (2008). Medline doi:10.1016/j.neuroimage.2008.06.037

40. A. A. Grace, Phasic versus tonic dopamine release and the modulation of dopamine system responsivity: A hypothesis for the etiology of schizophrenia. *Neuroscience* **41**, 1–24 (1991). Medline doi:10.1016/0306-4522(91)90196-U

41. P. N. Tobler, A. Dickinson, W. Schultz, Coding of predicted reward omission by dopamine neurons in a conditioned inhibition paradigm. *J. Neurosci.* **23**, 10402–10410 (2003). Medline

42. A. Ghazizadeh, F. Ambroggi, N. Odean, H. L. Fields, Prefrontal cortex mediates extinction of responding by two distinct neural mechanisms in accumbens shell. *J. Neurosci.* **32**, 726–737 (2012). Medline doi:10.1523/JNEUROSCI.3891-11.2012

43. M. D. Greicius, B. H. Flores, V. Menon, G. H. Glover, H. B. Solvason, H. Kenna, A. L. Reiss, A. F. Schatzberg, Resting-state functional connectivity in major depression: Abnormally increased contributions from subgenual cingulate cortex and thalamus. *Biol. Psychiatry* **62**, 429–437 (2007). Medline doi:10.1016/j.biopsych.2006.09.020

44. J. D. Berke, Functional properties of striatal fast-spiking interneurons. *Front. Syst. Neurosci.* **5**, 45 (2011). Medline doi:10.3389/fnsys.2011.00045

45. J. H. Lee, R. Durand, V. Gradinaru, F. Zhang, I. Goshen, D. S. Kim, L. E. Fenno, C. Ramakrishnan, K. Deisseroth, Global and local fMRI signals driven by neurons defined optogenetically by type and wiring. *Nature* **465**, 788–792 (2010). Medline doi:10.1038/nature09108

46. A. M. Aravanis, L. P. Wang, F. Zhang, L. A. Meltzer, M. Z. Mogri, M. B. Schneider, K. Deisseroth, An optical neural interface: In vivo control of rodent motor cortex with integrated fiberoptic and optogenetic technology. *J. Neural Eng.* **4**, S143–S156 (2007). Medline doi:10.1088/1741-2560/4/3/S02

47. H. W. Berendse, Y. Galis-de Graaf, H. J. Groenewegen, Topographical organization and relationship with ventral striatal compartments of prefrontal corticostriatal projections in the rat. *J. Comp. Neurol.* **316**, 314–347 (1992). Medline doi:10.1002/cne.903160305

48. C. Hamani, M. Diwan, C. E. Macedo, M. L. Brandão, J. Shumake, F. Gonzalez-Lima, R. Raymond, A. M. Lozano, P. J. Fletcher, J. N. Nobrega, Antidepressant-like effects of medial prefrontal cortex deep brain stimulation in rats. *Biol. Psychiatry* **67**, 117–124 (2010). Medline doi:10.1016/j.biopsych.2009.08.025

49. D. Chaudhury, J. J. Walsh, A. K. Friedman, B. Juarez, S. M. Ku, J. W. Koo, D. Ferguson, H. C. Tsai, L. Pomeranz, D. J. Christoffel, A. R. Nectow, M. Ekstrand, A. Domingos, M. S. Mazei-Robison, E. Mouzon, M. K. Lobo, R. L. Neve, J. M. Friedman, S. J. Russo, K. Deisseroth, E. J. Nestler, M. H. Han, Rapid regulation of depression-related behaviours by control of midbrain dopamine neurons. *Nature* **493**, 532–536 (2013). Medline doi:10.1038/nature11713

50. B. K. Lim, K. W. Huang, B. A. Grueter, P. E. Rothwell, R. C. Malenka, Anhedonia requires MC4R-mediated synaptic adaptations in nucleus accumbens. *Nature* **487**, 183–189 (2012). Medline doi:10.1038/nature11160

51. L. A. Gunaydin, L. Grosenick, J. C. Finkelstein, I. V. Kauvar, L. E. Fenno, A. Adhikari, S. Lammel, J. J. Mirzabekov, R. D. Airan, K. A. Zalocusky, K. M. Tye, P. Anikeeva, R. C.

Malenka, K. Deisseroth, Natural neural projection dynamics underlying social behavior. *Cell* **157**, 1535–1551 (2014). Medline doi:10.1016/j.cell.2014.05.017

52. J. Friedman, T. Hastie, R. Tibshirani, Sparse inverse covariance estimation with the graphical lasso. *Biostatistics* **9**, 432–441 (2008). Medline doi:10.1093/biostatistics/kxm045

53. T. Zhao, H. Liu, K. Roeder, J. Lafferty, L. Wasserman, The huge package for high-dimensional undirected graph estimation in R. *J. Mach. Learn. Res.* **13**, 1059–1062 (2012).

54. R. L. Bluhm, J. Miller, R. A. Lanius, E. A. Osuch, K. Boksman, R. W. Neufeld, J. Théberge, B. Schaefer, P. C. Williamson, Retrosplenial cortex connectivity in schizophrenia. *Psychiatry Res. Neuroimaging* **174**, 17–23 (2009). Medline doi:10.1016/j.pscychresns.2009.03.010

55. M. de la Iglesia-Vaya, M. J. Escartí, J. Molina-Mateo, L. Martí-Bonmatí, M. Gadea, F. X. Castellanos, E. J. Aguilar García-Iturrospe, M. Robles, B. B. Biswal, J. Sanjuan, Abnormal synchrony and effective connectivity in patients with schizophrenia and auditory hallucinations. *NeuroImage Clin.* **6**, 171–179 (2014). Medline doi:10.1016/j.nicl.2014.08.027

56. G. G. Gregoriou, S. J. Gotts, H. Zhou, R. Desimone, High-frequency, long-range coupling between prefrontal and visual cortex during attention. *Science* **324**, 1207–1210 (2009). Medline doi:10.1126/science.1171402

57. M. Siegel, T. H. Donner, A. K. Engel, Spectral fingerprints of large-scale neuronal interactions. *Nat. Rev. Neurosci.* **13**, 121–134 (2012). Medline

58. K. M. Igarashi, L. Lu, L. L. Colgin, M.-B. Moser, E. I. Moser, Coordination of entorhinal-hippocampal ensemble activity during associative learning. *Nature* **510**, 143–147 (2014). Medline doi:10.1038/nature13162

59. G. Buzsáki, X.-J. Wang, Mechanisms of gamma oscillations. *Annu. Rev. Neurosci.* **35**, 203–225 (2012). Medline doi:10.1146/annurev-neuro-062111-150444

60. G. Buzsáki, C. A. Anastassiou, C. Koch, The origin of extracellular fields and currents—EEG, ECoG, LFP and spikes. *Nat. Rev. Neurosci.* **13**, 407–420 (2012). Medline doi:10.1038/nrn3241

61. S. Ikemoto, Dopamine reward circuitry: Two projection systems from the ventral midbrain to the nucleus accumbens-olfactory tubercle complex. *Brain Res. Rev.* **56**, 27–78 (2007). Medline doi:10.1016/j.brainresrev.2007.05.004

62. S. N. Haber, B. Knutson, The reward circuit: Linking primate anatomy and human imaging. *Neuropsychopharmacology* **35**, 4–26 (2010). Medline doi:10.1038/npp.2009.129

63. T. W. Robbins, B. J. Everitt, Neurobehavioural mechanisms of reward and motivation. *Curr. Opin. Neurobiol.* **6**, 228–236 (1996). Medline doi:10.1016/S0959-4388(96)80077-8

64. B. Knutson, J. M. Bjork, G. W. Fong, D. Hommer, V. S. Mattay, D. R. Weinberger, Amphetamine modulates human incentive processing. *Neuron* **43**, 261–269 (2004). Medline doi:10.1016/j.neuron.2004.06.030

65. D. L. Robinson, B. J. Venton, M. L. Heien, R. M. Wightman, Detecting subsecond dopamine release with fast-scan cyclic voltammetry in vivo. *Clin. Chem.* **49**, 1763–1773 (2003). Medline doi:10.1373/49.10.1763

66. P. E. Phillips, D. L. Robinson, G. D. Stuber, R. M. Carelli, R. M. Wightman, "Real-time measurements of phasic changes in extracellular dopamine concentration in freely moving rats by fast-scan cyclic voltammetry," in *Drugs of Abuse: Neurological Reviews and Protocols*, J. Q. Wang, Ed. (Methods in Molecular Medicine Series, Humana Press, Totowa, NJ, 2003), pp. 443–464.

67. S. M. Nicola, J. Surmeier, R. C. Malenka, Dopaminergic modulation of neuronal excitability in the striatum and nucleus accumbens. *Annu. Rev. Neurosci.* **23**, 185–215 (2000). Medline doi:10.1146/annurev.neuro.23.1.185

68. B. Knutson, C. M. Adams, G. W. Fong, D. Hommer, Anticipation of increasing monetary reward selectively recruits nucleus accumbens. *J. Neurosci.* **21**, RC159 (2001). Medline

69. B. H. Schott, L. Minuzzi, R. M. Krebs, D. Elmenhorst, M. Lang, O. H. Winz, C. I. Seidenbecher, H. H. Coenen, H. J. Heinze, K. Zilles, E. Düzel, A. Bauer, Mesolimbic functional magnetic resonance imaging activations during reward anticipation correlate with reward-related ventral striatal dopamine release. *J. Neurosci.* **28**, 14311–14319 (2008). Medline doi:10.1523/JNEUROSCI.2058-08.2008

70. B. Knutson, S. E. B. Gibbs, Linking nucleus accumbens dopamine and blood oxygenation. *Psychopharmacology* **191**, 813–822 (2007). Medline doi:10.1007/s00213-006-0686-7

71. H.-S. Liu, S. Chefer, H. Lu, K. Guillem, W. Rea, P. Kurup, Y. Yang, L. Peoples, E. A. Stein, Dorsolateral caudate nucleus differentiates cocaine from natural reward-associated contextual cues. *Proc. Natl. Acad. Sci. U.S.A.* **110**, 4093–4098 (2013). Medline doi:10.1073/pnas.1207531110

72. G. D. Stuber, T. S. Hnasko, J. P. Britt, R. H. Edwards, A. Bonci, Dopaminergic terminals in the nucleus accumbens but not the dorsal striatum corelease glutamate. *J. Neurosci.* **30**, 8229–8233 (2010). Medline doi:10.1523/JNEUROSCI.1754-10.2010

73. K. T. Beier, E. E. Steinberg, K. E. DeLoach, S. Xie, K. Miyamichi, L. Schwarz, X. J. Gao, E. J. Kremer, R. C. Malenka, L. Luo, Circuit architecture of VTA dopamine neurons revealed by systematic input-output mapping. *Cell* **162**, 622–634 (2015). Medline doi:10.1016/j.cell.2015.07.015

74. N. Lally, A. C. Nugent, D. A. Luckenbaugh, R. Ameli, J. P. Roiser, C. A. Zarate, Anti-anhedonic effect of ketamine and its neural correlates in treatment-resistant bipolar depression. *Transl. Psychiatry* **4**, e469 (2014). Medline doi:10.1038/tp.2014.105

75. G. Juckel, F. Schlagenhauf, M. Koslowski, T. Wüstenberg, A. Villringer, B. Knutson, J. Wrase, A. Heinz, Dysfunction of ventral striatal reward prediction in schizophrenia. *Neuroimage* **29**, 409–416 (2006). Medline doi:10.1016/j.neuroimage.2005.07.051

76. E. C. Dowd, D. M. Barch, Anhedonia and emotional experience in schizophrenia: Neural and behavioral indicators. *Biol. Psychiatry* **67**, 902–911 (2010). Medline doi:10.1016/j.biopsych.2009.10.020

77. A. Lüthi, C. Lüscher, Pathological circuit function underlying addiction and anxiety disorders. *Nat. Neurosci.* **17**, 1635–1643 (2014). Medline doi:10.1038/nn.3849

78. M. E. Jackson, A. S. Frost, B. Moghaddam, Stimulation of prefrontal cortex at physiologically relevant frequencies inhibits dopamine release in the nucleus accumbens. *J. Neurochem.* **78**, 920–923 (2001). Medline doi:10.1046/j.1471-4159.2001.00499.x

79. H. E. Covington III, M. K. Lobo, I. Maze, V. Vialou, J. M. Hyman, S. Zaman, Q. LaPlant, E. Mouzon, S. Ghose, C. A. Tamminga, R. L. Neve, K. Deisseroth, E. J. Nestler, Antidepressant effect of optogenetic stimulation of the medial prefrontal cortex. *J. Neurosci.* **30**, 16082–16090 (2010). Medline doi:10.1523/JNEUROSCI.1731-10.2010

80. B. Giros, M. Jaber, S. R. Jones, R. M. Wightman, M. G. Caron, Hyperlocomotion and indifference to cocaine and amphetamine in mice lacking the dopamine transporter. *Nature* **379**, 606–612 (1996). Medline doi:10.1038/379606a0

81. L. K. Krugel, G. Biele, P. N. Mohr, S.-C. Li, H. R. Heekeren, Genetic variation in dopaminergic neuromodulation influences the ability to rapidly and flexibly adapt decisions. *Proc. Natl. Acad. Sci. U.S.A.* **106**, 17951–17956 (2009). Medline doi:10.1073/pnas.0905191106

82. Full details of the materials and methods are available as supplementary materials on *Science* Online.

83. G. H. Glover, C. S. Law, Spiral-in/out BOLD fMRI for increased SNR and reduced susceptibility artifacts. *Magn. Reson. Med.* **46**, 515–522 (2001). Medline doi:10.1002/mrm.1222

84. C. S. Law, G. H. Glover, Interleaved spiral-in/out with application to functional MRI (fMRI). *Magn. Reson. Med.* **62**, 829–834 (2009). Medline doi:10.1002/mrm.22056

85. C. Chang, G. H. Glover, Variable-density spiral-in/out functional magnetic resonance imaging. *Magn. Reson. Med.* **65**, 1287–1296 (2011). Medline doi:10.1002/mrm.22722

86. G. T. Buračas, G. M. Boynton, Efficient design of event-related fMRI experiments using M-sequences. *Neuroimage* **16**, 801–813 (2002). Medline doi:10.1006/nimg.2002.1116

87. G. H. Glover, Deconvolution of impulse response in event-related BOLD fMRI. *Neuroimage* **9**, 416–429 (1999). Medline doi:10.1006/nimg.1998.0419

88. M. R. Warden, A. Selimbeyoglu, J. J. Mirzabekov, M. Lo, K. R. Thompson, S. Y. Kim, A. Adhikari, K. M. Tye, L. M. Frank, K. Deisseroth, A prefrontal cortex-brainstem neuronal projection that controls response to behavioural challenge. *Nature* **492**, 428–432 (2012). Medline

89. J. A. King, T. S. Garelick, M. E. Brevard, W. Chen, T. L. Messenger, T. Q. Duong, C. F. Ferris, Procedure for minimizing stress for fMRI studies in conscious rats. *J. Neurosci. Methods* **148**, 154–160 (2005). Medline doi:10.1016/j.jneumeth.2005.04.011

90. R. W. Cox, AFNI: Software for analysis and visualization of functional magnetic resonance neuroimages. *Comput. Biomed. Res.* **29**, 162–173 (1996). Medline doi:10.1006/cbmr.1996.0014

91. S. D. Forman, J. D. Cohen, M. Fitzgerald, W. F. Eddy, M. A. Mintun, D. C. Noll, Improved assessment of significant activation in functional magnetic resonance imaging (fMRI): Use of a cluster-size threshold. *Magn. Reson. Med.* **33**, 636–647 (1995). Medline doi:10.1002/mrm.1910330508

92. F. Pedregosa *et al*., Scikit-learn: Machine learning in Python. *J. Mach. Learn. Res.* **12**, 2825–2830 (2011).

93. N. Meinshausen, P. Bühlmann, Stability selection. *J. R. Stat. Soc. Ser. B* **72**, 417–473 (2010). doi:10.1111/j.1467-9868.2010.00740.x

94. G. Paxinos, C. Watson, *The Rat Brain in Stereotaxic Coordinates* (Academic Press, San Diego, ed. 4, 1998).

95. H. Bokil, P. Andrews, J. E. Kulkarni, S. Mehta, P. P. Mitra, Chronux: A platform for analyzing neural signals. *J. Neurosci. Methods* **192**, 146–151 (2010). Medline doi:10.1016/j.jneumeth.2010.06.020